A Tale of Twins: The Distinct Roles of Intracellular and Extracellular Formate in Regulating Flagellar and Pathogenicity Island-1 Genes in *Salmonella* Typhimurium

Debapriya Mukherjee[1], Dipshikha Chakravortty[1,2*]

[1]Department of Microbiology and Cell Biology, Division of Biological Sciences, Indian Institute of Science, Bangalore, India.

[2]School of Biology, Indian Institute of Science Education and Research, Thiruvananthapuram, 695551.

[*]Corresponding author: dipa@iisc.ac.in

Tel: 0091 80 2293 2842

Fax: 0091 80 2360 2697

Abstract

Host-derived short-chain fatty acids (SCFAs) are extensively being studied for their role in the virulence and pathogenesis of *Salmonella* Typhimurium (STM). Formate, an SCFA present in the ileum, functions as a signalling molecule to enhance STM invasion. However, the role of intracellular formate in *Salmonella* virulence remains poorly understood. To investigate this, we generated knockouts of *pflB* (pyruvate-formate lyase) and *focA* (formate transporter). Disruption of formate production through *pflB* deletion led to reduced flagellation and increased *hilA* and *prgH* expression, attributed to elevated intracellular pH and membrane damage. This suppression of flagellar machinery drives a shift from adhesion to invasion, regulated by RpoE via the CsrA/*csrB* pathway. Additionally, we demonstrate that upon compensation for intracellular deficiency of formate, STM *ΔpflB* starts to utilize formate as a signalling molecule to regulate downstream processes. To the best of our knowledge, this study is the first to establish the critical role of the *pflB* gene in maintaining intracellular pH and controlling virulence gene expression in STM. Lastly, our findings emphasize the importance of modulating *pflB* expression across intestinal regions to optimize STM invasion.

Keywords: Flagella/ Formate/ Intracellular pH/ Membrane depolarization/ Short Chain Fatty Acids (SCFAs)

Introduction

The genus *Salmonella* consists of Gram-negative gammaproteobacteria that infect a wide range of human and animal hosts [1]. Non-typhoidal serovars, such as *Salmonella* Typhimurium, are commonly associated with self-limiting diarrheal illness with relatively low fatality. According to the Global Burden of Diseases, Injuries, and Risk Factors Study (GBD) 2017, there were an estimated 95.1 million cases of *Salmonella* enterocolitis worldwide, resulting in 50,771 deaths [2-4]. Although non-typhoidal infections are typically confined to the intestines, these serovars can occasionally invade sterile tissues, leading to bacteraemia, meningitis, and other focal infections, which significantly increase mortality rates.[5].

Salmonella Typhimurium enters the host via contaminated food and water. One of the defence mechanisms in the host is the presence of short-chain fatty acids (SCFAs) in the small intestine. SCFAs are produced through the anaerobic fermentation of non-digestible polysaccharides, such as resistant starches and dietary fibres. The SCFAs found in the intestine—formate (C1), acetate (C2), propionate (C3), and butyrate (C4), with concentrations reaching up to 10–100 mM. Recent studies have extensively explored the role of SCFAs ((like butyrate and propionate) in *Salmonella* infections [6-10]. For example, butyrate downregulates the expression of pathogenicity island-1 (SPI-1) genes in *S.* Typhimurium, thereby reducing bacterial invasion and translocation from the intestines to the bloodstream [11-13].

Formate present in the intestine has been previously shown to act as a diffusible signal promoting *Salmonella* Typhimurium invasion. [14]. Imported, unmetabolized formic acid functions as a cytoplasmic signal by binding to HilD, the master transcriptional regulator of *Salmonella* invasion, thereby preventing inhibitory fatty acids from binding and extending the

activity of HilD, which leads to the derepression of invasion genes [15]. Moreover, formate utilization by respiratory enzymes such as formate dehydrogenase-N (FdnGHI) and formate dehydrogenase-O (FdoGHI) plays a key role in *Salmonella* colonization of the gut [16]. *S.* Typhimurium can source formate from both its own pyruvate-formate lyase (PflB) and from the intestinal environment [17, 18]. However, the role of endogenously produced formate in regulating *Salmonella* virulence and pathogenesis have seldom been reported [19].

In this study, we examined the role of endogenously produced formate in the pathogenic lifestyle of *S.* Typhimurium. To the best of our knowledge, we are the first to identify the role of the *pflB* gene in regulating cytosolic pH of STM, which is instrumental in maintaining the flagellar operon. Quite interestingly, in the wild-type strain with an intact formate pool, extracellular formate functions as a signalling molecule via the BarA/SirA two-component system, highlighting the distinct roles of intracellular and extracellular formate pools in regulating *Salmonella* virulence. We demonstrate that regulating the *pflB* gene in various regions of the intestine may be a strategy utilized by *Salmonella* to optimize its invasion of the distal ileum, its primary target site.

Materials and Methods

Bacterial strains and plasmids

The wild-type *Salmonella enterica* subspecies *enterica* serovar Typhimurium strain 14028S used in this study was generously provided by Professor Michael Hensel from the Max von Pettenkofer Institute for Hygiene and Medical Microbiology, Germany. Knockout and complement strains were generated specifically for this study. Bacterial strains were stored as glycerol stocks at -80°C and revived on fresh Luria-Bertani (LB) agar plates (HiMedia) with appropriate antibiotics as needed (50 µg/ml Kanamycin, 50 µg/ml Ampicillin, 25 µg/ml

Chloramphenicol). A single colony was inoculated into a fresh LB tube with antibiotics when required and incubated at 37°C with shaking (170 rpm) to obtain an overnight culture. Strains containing the pKD46 plasmid were incubated overnight at 30°C with shaking (170 rpm). A complete list of bacterial strains and plasmids used in this study is provided in Table 1.

Construction of the knockout strains of *Salmonella*

The knockout strains of *Salmonella* were generated using the one-step chromosomal gene inactivation technique developed by Datsenko and Wanner [20]. In brief, STM (WT) was transformed with the pKD46 plasmid, which expresses the λ-Red recombinase system under the control of an arabinose-inducible promoter. Transformed cells were selected on LB plates containing 50 µg/ml Ampicillin. To generate the knockout strains, a single colony of STM (WT)/pKD46 was inoculated into fresh LB medium with 50 µg/ml Ampicillin and 50 mM arabinose, then incubated overnight at 30°C with shaking (170 rpm). The overnight culture was then subcultured into fresh LB medium and incubated under the same conditions for 2.5 hours to reach an OD_{600} of 0.35-0.4. Electrocompetent STM (WT)/pKD46 cells were prepared by washing the bacterial pellet with chilled, autoclaved MilliQ water and 10% glycerol. Kanamycin (KanR, 1.5 kb) and Chloramphenicol (ChlR, 1.1 kb) resistance cassettes were amplified from pKD4 and pKD3 plasmids, respectively, using knockout-specific primers. The amplified resistance cassettes were then electroporated into STM (WT)/pKD46, and transformed cells were selected on LB agar plates with the appropriate antibiotics (Kanamycin or Chloramphenicol). Knockout colonies were confirmed using gene-specific intragenic primers, knockout confirmatory primers, and antibiotic-cassette-specific primers.

For generating double-knockout strains, the one-step chromosomal gene inactivation method was slightly modified. Briefly, STM Δ*pflB* was transformed with the pKD46 plasmid. An

113 overnight culture of the transformed strain was subcultured into fresh LB medium
114 supplemented with 50 mM arabinose and 50 µg/ml Ampicillin, then incubated at 30°C with
115 shaking (170 rpm) for 2.5 hours until it reached an OD600 of 0.3-0.4. The chloramphenicol
116 resistance cassette (1.1 kb), flanked by regions homologous to *focA*, was electroporated into
117 electrocompetent STM Δ*pflB*/pKD46 cells to generate STM Δ*focA*Δ*pflB*. The double-knockout
118 strains were selected on LB agar plates containing Kanamycin (50 µg/ml) and
119 Chloramphenicol (25 µg/ml). These double-knockout colonies were further confirmed with
120 knockout confirmatory and gene-specific intragenic primers. The primers used for generating
121 knockouts are listed in Table 2.

122

123 Construction of complemented and overexpression strains of *Salmonella*

124 The *pflB* and *csrA* genes were amplified from the genomic DNA of wild-type *Salmonella* using
125 gene-specific cloning primers. Both the colony PCR products and the empty pQE60 cloning
126 vector were digested with BamHI-HF and HindIII-HF (NEB) at 37°C for 1 hour. After double
127 digestion, the insert and vector were purified and ligated using T4 DNA Ligase (NEB) at 16°C
128 overnight. The ligation product was then transformed into *Escherichia coli* TG1 using the heat
129 shock method. Successful cloning was confirmed by double digestion of the recombinant
130 plasmid. The confirmed recombinant plasmid was subsequently transformed into *Salmonella*
131 strains to create complemented and overexpression strains. Primers used for generating
132 complement strains are listed in Table 2.

133

134

135 RNA Isolation and RT-qPCR

136 Logarithmic-phase cultures of bacterial cells was centrifuged at 6,000 rpm at 4°C, and the
137 resulting pellet was resuspended in TRIzol reagent. The suspension was stored at -80°C until
138 further use. RNA was isolated from the lysed supernatants using the chloroform-isopropanol
139 method. The RNA pellet was washed with 70% ethanol and resuspended in 30 µl of DEPC-
140 treated MilliQ water. RNA concentration was measured with a NanoDrop spectrophotometer
141 (Thermo Fisher Scientific), and quality was assessed on a 2% agarose gel. Following this, 2 µg
142 of RNA was treated with DNase using DNase TURBO (Thermo Fisher Scientific) at 37°C for
143 30 minutes. DNase was inactivated by adding 5 mM Na_2EDTA (Thermo Fisher Scientific) and
144 incubating at 65°C for 10 minutes. cDNA synthesis was carried out using the PrimeScript RT
145 reagent kit (Takara, CAT RR037A) according to the manufacturer's instructions. Quantitative
146 real-time PCR (qRT-PCR) was performed with a TB Green RT-qPCR kit (Takara) on the
147 QuantStudio 5 Real-Time PCR system. Intragenic primers were used to examine gene
148 expression, and expression levels were normalized to 16S rRNA. Primer sequences are listed
149 in Table 2.

150

151

152 Eukaryotic cell lines and growth conditions

153 The HeLa, Caco-2, HepG2, and RAW 264.7 cell lines were cultured in Dulbecco's Modified
154 Eagle's Medium (DMEM, Sigma-Aldrich) supplemented with 10% Fetal Calf Serum (FCS,
155 Gibco), at 37°C with 5% CO_2.

156 Gentamicin Protection Assay and Intracellular Cell Survival Assay

157 Caco-2 and RAW 264.7 cells were seeded into tissue culture-treated 24-well plates. For
158 infection of the epithelial Caco-2 cells, overnight cultures of STM WT, STM Δ*pflB*, STM

159 Δ*pflB*/pQE60:*pflB*, and STM Δ*focAΔpflB* were subcultured in fresh LB medium, with or
160 without supplementation of 40 mM sodium formate (Sigma). For infection of the macrophage
161 cell line RAW 264.7, the overnight cultures were used directly. Both cell types were infected
162 at a multiplicity of infection (MOI) of 10. The plates were centrifuged at 1000 rpm for 10
163 minutes, after which the cells were incubated at 37°C with 5% CO_2 for 25 minutes. Following
164 incubation, cells were washed with 1X phosphate-buffered saline (PBS) to remove
165 extracellular, non-adherent, and loosely adherent bacteria, and fresh media containing 100
166 µg/ml gentamicin was added. After a 1-hour incubation, cells were washed again with 1X PBS
167 and exposed to 25 µg/ml gentamicin until lysis. Cell lysis was performed at 2 hours and 16
168 hours post-infection using 0.1% Triton X-100, and the lysates were plated onto *Salmonella-*
169 *Shigella* (SS) agar alongside the pre-inoculum. The percent invasion and fold proliferation were
170 determined using the following formulas:

171 **Percent invasion/phagocytosis= [C.F.U at 2h/ C.F.U of Pre-Inoculum] *100**

172 **Fold proliferation= [C.F.U at 16h/ C.F.U of 2h]**

173

174 Adhesion assay

175 The adhesion assay was performed by modifying the previously reported protocol [21].
176 Overnight cultures (12 hours old) of STM WT, STM *ΔpflB*, and STM *ΔfliC* were subcultured
177 into fresh LB medium, with or without supplementation of 40 mM sodium formate (Sigma).
178 The logarithmic phase of these bacterial strains was used to infect the cells at a multiplicity of
179 infection (MOI) of 10. The plates were centrifuged at 1000 rpm for 10 minutes, followed by
180 incubation at 37°C with 5% CO_2 for 10 minutes. To remove extracellular, unadhered, and
181 loosely adhered bacteria, the cells were washed twice with 1X phosphate-buffered saline
182 (PBS). Subsequently, the cells were lysed with 0.1% Triton X-100, and the lysates were plated

183 on Salmonella-Shigella (SS) agar alongside the pre-inoculum. The percent adhesion was
184 determined using the following formula:

185 **Percent adhesion= [C.F.U at 10 mins Post Infection/ C.F.U of Pre-Inoculum] *100**

186

187 TEM

188 Transmission Electron Microscopy was performed by modifying the protocol by Marathe *et al*
189 [22]. In brief, overnight cultures of STM WT, STM *ΔpflB*, STM *ΔfocA*, STM *ΔfocAΔpflB*, STM
190 WT/*csrA*, STM *ΔpflB*/*csrA*, STM *ΔrpoE*, and STM *ΔpflBΔrpoE* were subcultured (1:100) in
191 fresh LB medium, with or without supplementation (+/-F), and incubated at 37°C for 2.5–3
192 hours under shaking conditions. The bacterial samples were then washed twice with 1X
193 phosphate-buffered saline (PBS) and resuspended in 50 µl of 1X PBS. A 5 µl aliquot of the
194 suspension was applied to a glow-discharged copper grid and allowed to air-dry. The bacteria
195 were subsequently negatively stained using 1% uranyl acetate. After air-drying, the samples
196 were imaged using Transmission Electron Microscopy (JEM-100 CX II; JEOL).

197 Confocal Microscopy

198 Confocal Microscopy was performed by modifying the protocol by Marathe *et al* [22]. In
199 summary, 12-hour-old stationary-phase cultures of STM WT, STM *ΔpflB*, STM *ΔfocAΔpflB*,
200 STM WT/*csrA*, STM *ΔpflB*/*csrA*, STM *ΔrpoE*, and STM *ΔpflBΔrpoE*, with or without
201 supplementation (+/-F), were subcultured (1:100) into fresh LB medium and incubated at 37°C
202 for 2.5–3 hours under shaking conditions until reaching the logarithmic phase. A 100 µl aliquot
203 of the log-phase culture was spotted onto sterile coverslips and air-dried overnight. Once
204 completely dried, the samples were fixed with 3.5% paraformaldehyde (PFA). The PFA was
205 washed off with 1X PBS, and the samples were stained with a rabbit-raised anti-Fli primary

206 antibody (1:100 dilution in 2.5% BSA solution, Difco) for 3 hours at room temperature. After
207 washing off the primary antibody with 1X PBS, the samples were incubated with Alexa-488-
208 conjugated anti-rabbit secondary antibody (Sigma) for 45 minutes at room temperature. Before
209 mounting the coverslips onto clean glass slides, the samples were stained with DAPI (4',6-
210 diamidino-2-phenylindole) at 100 µg/ml for 5 minutes. The coverslips were sealed with
211 transparent nail polish. All images were captured using a Zeiss 880 microscope and analyzed
212 with Zeiss ZEN Black 2012 software.

213 Gas Chromatography-Mass Spectrometry

214 GC-MS was performed by modifying the protocol by Hughes *et al* [23]. Briefly, overnight
215 cultures of STM WT, STM *ΔpflB*, STM *ΔfocA*, STM *ΔfocAΔpflB* were subcultured (1:100) into
216 100 ml of LB Broth. After 2.5-3h of incubation at 37˚C under shaking conditions, 50 ml of the
217 individual cultures were centrifuged at 6,000 rpm for 10 mins. The pellet was washed twice
218 with 1X PBS to remove the remnants of the media. Finally, the pellet was resuspended in 1 ml
219 of 1X PBS, and the suspension was sonicated to lyse the bacterial cells. The cell debris was
220 removed by centrifugation. Before sonication, the CFU in the pellet had been recorded by
221 plating.

222 Sodium formate (Sigma) was used as an external standard. External standards and biological
223 samples were derivatized before the Mass Spectrometry. 2 M hydrochloric acid was added in
224 a 1:1 ratio to the samples to protonate formate. Liquid-liquid extraction was done which
225 extracted formic acid into ethyl acetate (Sigma-Aldrich). To remove any remaining water, the
226 ethyl acetate extract was passed through a column of anhydrous sodium sulfate (Sigma-
227 Aldrich). The ethyl acetate extract of formic acid was then incubated at 80 ºC for 1 h with the
228 derivatization reagent N, O-Bis(trimethylsilyl)trifluoro acetamide (Sigma Aldrich) with 1%
229 Chlorotrimethylsilane (Fluka). The derivatized samples were then transferred to autosampler

230 vials for analysis by Gas Chromatography Mass Spectrometry (Agilent technologies, 7890A
231 GC, 5975C MS). The injection temperature was set to 200 °C and the injection split ratio was
232 1:40 with an injection volume of 1 µL. The oven temperature was set to start at 40 °C for 4
233 min, with an increase to 120 °C at 5 °C per min and to 200 °C at 25 °C per min with a final
234 hold at this temperature for 3 min. Helium carrier gas had a flow rate of 1.2mL/min with
235 constant flow mode. A 30 m × 0.25 mm × 0.40 µm DB-624 column from Agilent was used.
236 The interface temperature was set to 220 °C. The electron impact ion source temperature was
237 at 230 °C, with an ionization energy of 70 eV and 1235 EM volts. For qualitative experiments,
238 selected ion monitoring (single quadrupole mode) of 103 m/z scan had been performed. The
239 retention time for formate and deuterated formate was 5.9 min. The target and reference
240 (qualifier) ions for formate were m/z = 103 and m/z = 75, respectively. The formate
241 concentration of each sample was interpolated from a standard curve with the known standards.
242 It was normalized with the CFU values of each sample to obtain the intracellular formate
243 concentration/CFU.

244 To determine the formate transportation into the cell, we subcultured overnight cultures of STM
245 WT, STM *ΔpflB*, STM *ΔfocA*, and STM *ΔfocAΔpflB* into fresh LB tubes. During the subculture,
246 Sodium Formate was supplemented into each tube to maintain a concentration of 1M. Post 2.5-
247 3h of incubation at 37˚C under shaking conditions, the bacterial cells were removed from the
248 media by centrifuging the culture twice at 6,000 rpm for 10 mins. A 2 µm filter was used to
249 remove any other bacterial cells left in the spent media. Following this, a similar protocol as
250 mentioned above was used to quantify the residual formate in the spent media. It was compared
251 to the media where bacterial cells had not been subcultured.

252

253 **Bisbenzimide Assay**

254 The bisbenzimide assay was performed by modifying the protocol by Roy Chowdhury *et al*
255 [24]. Briefly, overnight cultures of STM WT, STM *ΔpflB*, and STM *ΔfliC* were subcultured
256 into fresh LB tubes(+/-F). Logarithmic phase cultures of each condition were taken and the
257 OD_{600} was adjusted to 0.1. To 180 µl of this bacterial suspension, 20 µl of Bisbenzimide dye
258 (10µg/ml) was added. It was incubated at 37˚C for 10 mins. The intracellular DNA-bound
259 bisbenzimide was quantified in a TECAN 96 well microplate reader using a 346 nm excitation
260 and 460 nm emission filter.

261

262 **Staining with $DiBAC_4$**

263 The $DiBAC_4$ staining was performed by modifying the protocol by Roy Chowdhury *et al* [25].
264 Membrane potential or membrane porosity was quantified by using a membrane potential
265 sensitive fluorescent dye bis-(1,3-dibutyl barbituric acid)- trimethylene oxonol (Invitrogen).
266 For this purpose, overnight culture of STM WT, STM *ΔpflB*, and STM *ΔfliC* were subcultured
267 with or without the supplementation of 40 mM Sodium Formate (Sigma). Around $4.5*10^7$ cells
268 of the logarithmic phase culture were incubated with 1 µg/ml of $DiBAC_4$ dye at 37˚C for 30
269 mins. The percentage of $DiBAC_4$-positive cells and the Median Fluorescence Intensity (MFI)
270 of $DiBAC_4$ was determined by flow cytometry (BD FACSVerse by BD Biosciences-US).

271

272 **BCECF-AM Staining**

273 The BCECF-AM staining was performed by modifying the protocol by Roy Chowdhury *et al*
274 [24]. The acidification of the cytosol with the change in pH of extracellular conditions was
275 determined using a cell-permeable dual excitation ratiometric dye 2',7'-Bis-(2-Carboxyethyl)-
276 5- (and-6)-Carboxyfluorescein, Acetoxymethyl Ester (BCECF-AM). Briefly, the logarithmic

277 phase cultures of STM WT, STM *ΔpflB* (+/-F) were resuspended in buffers of different pH
278 (5,5.5,6,7). They were incubated for 2 hours at 37˚C before the addition of 1 mg/ml BCECF-
279 AM to make a final concentration of 20 µM. The cells were incubated with the dye for 30
280 minutes. Post-incubation, the cells were analysed by flow cytometry (BD FACSVerse by BD
281 Biosciences, US) with 488 nm and 405 nm excitation and 535 nm excitation channels. The
282 MFI of the bacterial cells at 488 nm and 405 nm was obtained from BD FACSuite software
283 and the ratio of 488/405 was utilized to determine the cytosolic acidification in response to
284 changing pH conditions.

285

286 Intracellular pH measurement by pHuji plasmid

287 STM WT and STM *ΔpflB* were transformed with the plasmid pBAD:pHuji (Plasmid #61555)
288 that encodes a pH-sensitive red fluorescent protein pHuji [26, 27]. The logarithmic cultures of
289 STM WT/pBAD:pHuji and STM *ΔpflB*/pBAD:pHuji (+/-F) were incubated in phosphate
290 buffers of pH 5,6,7,8,9 in the presence of 40 µM Sodium Benzoate to equilibrate the
291 intracellular pH with the extracellular one. The resultant fluorescent intensity was plotted as a
292 function of pH and was fitted to obtain a standard curve. The fluorescence values obtained from
293 LB-grown cultures of the bacterial cells (+/- F) were interpolated in the standard curve to obtain
294 the intracellular pH of the bacterial cells *in-vitro*.

295

296 Ethics Statement for Animal Experiments

297 All the animal experiments have been approved by the Institutional Animal Ethics Clearance
298 Committee (IAEC), Indian Institute of Science, Bangalore. The registration number is
299 48/1999/CPCSEA. The guidelines formulated by the Committee for the Purpose of Control

300 and Supervision of Experiments on Animals (CPCSEA) were strictly followed. The ethical
301 clearance number for this study is CAF/Ethics/853/2021.

302

303 Mice Survival Assay

304 6-8 weeks old male C57BL/6 mice and Balb/c mice were acquired from the specific-pathogen
305 free conditions of Central Animal Facility, IISc. To draw a comparison between the mortality
306 rate of WT and mutant strains, the mice (n=10) were orally gavaged with 10^8 cells from the
307 stationary phase culture of each. After infection, mice were monitored every day for survival,
308 and the data was represented as percent survival.

309

310 Determination of bacterial burden in different organs

311 To understand the organ burden of the WT and mutant strain post-infection in mice, 10^7 cells
312 from the overnight culture of the bacterial strains were orally gavaged into 6-8 weeks old
313 C57BL/6 mice. 5 days post-infection, the mice were ethically euthanized, and the liver, spleen,
314 and brain were acquired. The organs were homogenized, and appropriate dilutions of the
315 homogenate were plated on *Salmonella-Shigella* (SS Agar). The data was represented was
316 $\log_{10}$CFU/gm-wt.

317

318 Invasion Assay in mice

319 Invasion assay in mice was performed by modifying the protocol by Chandra *et al* [28]. Briefly,
320 10^7 cells from the overnight culture of the bacterial cells were orally gavaged into 6-8 weeks
321 old male C57BL/6 mice. 6 hours post-infection, the mice were ethically euthanized, and the

intestine was acquired. It was homogenized, and appropriate dilutions of the homogenate were plated on *Salmonella-Shigella* (SS Agar). Corresponding fecal matter was also collected, and it was also plated post homogenization. The data was represented was $\log_{10}$CFU/gm-wt.

Intraperitoneal infection of mice

Intraperitoneal infection of mice was performed with 10^3 CFU from the overnight cultures of WT and mutant strains. 2 days post-infection, the mice were ethically euthanized, and the liver and the spleen were obtained. The organ burden of the bacterial strains was determined by the same protocol as above.

Statistical Analysis

Each experiment has been repeated 1 to 8 times independently as mentioned in the figure legends. The statistical analyses were performed by a unpaired Student's t-test or two-way ANOVA multiple comparison test as denoted in the figure legends. The data obtained from the mice experiments were analyzed using the Mann-Whitney *U* test. The *p*-values below 0.05 were considered significant. The results are indicated as Mean ± SD or Mean ± SEM as mentioned in the figure legends. All the data were plotted and analysed using GraphPad Prism 8.4.2.

Results

343 **The deletion of the *pflB* gene led to decreased invasion efficiency in the Caco-**
344 **2 cell line, which corresponded to a reduced organ burden in C57BL/6 mice**
345 **five days after infection through oral gavaging**

346 To investigate the role of endogenous formate levels in *Salmonella* virulence and pathogenesis,
347 we created knockout strains of *pflB* and *focA* using the one-step gene inactivation technique
348 outlined by Datsenko and Wanner [20]. FocA is the formate transporter in *Salmonella*
349 Typhimurium that functions as a passive export channel at high external pH and switches to an
350 active importer of formate at low pH [29]. The deletion of either gene did not impact the *in*
351 *vitro* growth of *Salmonella* in either complex LB media or M9 Minimal Media (**Figure S1 A-**
352 **B**). Since the *focA* and *pflB* genes are part of the same operon, we investigated whether deleting
353 one gene affected the expression of the other [30]. Our study revealed that deleting the upstream
354 *focA* gene resulted in decreased expression of the downstream *pflB* gene (**Figure S1C**).
355 However, deletion of *pflB* increased the expression of *focA* (**Figure S1D**).

356 To confirm that deleting *pflB* and *focA* indeed depleted the native formate pool of the cell, we
357 collected lysates from logarithmic phase cultures of all strains and quantified the formate
358 concentration using Gas Chromatography-Mass Spectrometry (GC-MS). After normalizing by
359 CFU, we observed that there was a significant reduction in the relative intracellular formate
360 concentrations upon deletion of *pflB*, whereas deletion of *focA* did not cause a notable change.
361 There was a significantly reduced intracellular formate level in STM *ΔfocAΔpflB* (**Figure 1A**).
362 This finding suggested the possibility of an alternative formate transporter. To investigate
363 further, we incubated secondary cultures of all strains in formate-supplemented media and
364 measured formate concentration in the spent media after 3 hours by GC-MS. We found a
365 significant reduction in formate concentration in the spent media of STM *ΔfocA* compared to
366 the control, indicating the presence of an alternative formate importer (**Figure 1B**). Since STM

367 Δ*focA* retained intracellular formate levels similar to STM WT and our data suggested the
368 presence of an alternate formate transporter, we focused our study on STM Δ*pflB*, where we
369 could successfully deplete the intracellular formate pool.

370 Intracellular Cell Survival Assay (ICSA) using the human colorectal carcinoma cell line Caco-
371 2 showed that STM *ΔpflB* exhibited reduced invasion efficiency compared to STM WT, but it
372 had similar fold proliferation to the latter (**Figure 1C**). The invasion deficiency in STM *ΔpflB*
373 was also rescued by complementing the gene with an exogenous pQE60 plasmid (**Figure S1E**).

374 In the murine macrophage cell line RAW 264.7, STM *ΔpflB* showed a decreased phagocytosis
375 and hyperproliferation compared to STM WT (**Figure 1E, F**).

376 To determine if the invasion deficiency observed in STM *ΔpflB* was consistent in an animal
377 model, we orally gavaged 10^7 CFU of STM WT and STM Δ*pflB* into 6–8-week-old male
378 C57BL/6 mice. Adhesion-deficient STM *ΔfliC* served as a control. Six hours post-infection,
379 we observed a reduced bacterial load in the mouse intestine for STM Δ*pflB*, which was
380 associated with increased faecal shedding compared to STM WT (**Figure 1G, H, I**). These
381 findings were consistent with the results for the control strain STM *ΔfliC*, which is known to
382 have reduced adhesion and is cleared more rapidly from the host [31].

383 To further understand the role of *pflB* deletion in overall *Salmonella* pathogenesis in *in-vivo*
384 mouse model, we orally gavaged 10^7 CFU of bacteria in 6-8 weeks old male C57BL/6 mice
385 and euthanized the mice 5 days post-infection (dpi) to determine the bacterial burden in the
386 liver, the spleen, and the brain (**Figure 1J, K, L**). We found a significantly reduced bacterial
387 burden in the liver and the spleen when infected with STM *ΔpflB* as compared to infection with
388 STM WT (**Figure 1K, L**). We also found that C57BL/6 mice infected with STM *ΔpflB* had a
389 better survival rate as compared to mice infected with STM WT (**Figure 1M**). We subjected
390 C57BL/6 mice to an intra-peritoneal infection with 10^3 CFU of both the WT and the knockout

391 strains. Under these conditions, we observed no significant change in the organ burden of STM
392 WT and STM *ΔpflB* 3dpi (**Figure S2A-D**). All these data suggested that the reduced organ
393 burden of STM *ΔpflB* upon oral gavaging is due to its attenuated adhesion in the gastrointestinal
394 tract, which promoted a faster clearance from the host body.

395

396 STM *ΔpflB* was deficient in flagella and the deficiency was partially 397 recovered upon supplementation of 40 mM sodium formate

398 *Salmonella* Typhimurium uses adhesins, such as flagella, to attach to host cells during infection
399 [32-34]. Following successful adhesion, it employs the *Salmonella* Pathogenicity Island-1
400 (SPI-1) machinery to invade non-phagocytic epithelial cells [35-37]. Our previous findings
401 indicated that STM Δ*pflB* has reduced invasion efficiency in Caco-2 cells. We opted to proceed
402 by supplementing exogenous formate to STM *ΔpflB* to determine whether the effects observed
403 from depleting intracellular formate could indeed be reversed through the addition of
404 extracellular formate. In our further studies, we used a concentration of 40 mM (indicated as F
405 henceforth), as it yielded maximal expression of the SPI-1 regulatory gene *hilA* in STM WT in
406 a concentration-dependent analysis ranging from 0 to 50 mM (**Figure S3A**). Interestingly, we
407 observed that STM Δ*pflB* exhibited increased expression of *prgH*, which encodes a structural
408 protein of the SPI-1 apparatus (**Figure 2A**). This expression was further elevated in STM
409 *ΔpflB*+F. Additionally, STM WT+F showed significantly higher *prgH* expression compared to
410 STM WT, consistent with the findings of Huang *et al* [17].

411 We also found that STM *ΔpflB* had lower *fliC* expression, which was partially restored under
412 +F conditions. Formate supplementation reduced *fliC* expression in STM WT as well,
413 compared to the untreated control (**Figure 2B**). We confirmed this via Transmission Electron
414 Microscopy (TEM) as well, where we found that STM WT+F had lesser flagella compared to

415 untreated control. STM *ΔpflB* had a reduced flagellar number, which was partially restored
416 upon supplementation of F (**Figure 2C**). Quantitative analysis of normalized MFI in confocal
417 microscopy and adhesion assays in the Caco-2 cell line further validated the findings from qRT-
418 PCR and TEM (**Figure 2 D-F**). STM WT+F also showed lesser motility on swim agar plate
419 compared to STM WT, however, we did not see a recovery in motility of STM *ΔpflB* upon F
420 supplementation (**Figure 2 G**). This indicates that while F supplementation in STM *ΔpflB* may
421 restore the transcription level of *fliC* and its protein expression, it does not lead to a recovery
422 in flagella-mediated motility. The partially restored adhesion observed in STM Δ*pflB*+F in the
423 Caco-2 cell line could be attributed to the increased surface hydrophobicity of the flagellar
424 filaments, resulting from the recovery in protein levels. This enhanced hydrophobicity
425 promotes stronger interactions for effective adhesion to eukaryotic host cells [38]. F
426 supplementation in STM *ΔpflB* was also associated with an improved invasion in Caco-2 cell
427 line. Complementation of the *pflB* via an extragenous plasmid in STM *ΔpflB* also led to an
428 improved percent invasion compared to the knockout strain. In line with our previous data, we
429 also found that STM WT+F had a higher percent invasion compared to STM WT (**Figure 2H**).

430 Further experimentation involved incubating secondary cultures of STM WT and STM Δ*pflB*
431 in varying concentrations of formate. Notably, formate significantly inhibited *fliC* expression
432 in STM WT starting from a concentration of 1 mM, while a concentration as low as 0.125 mM
433 was sufficient to restore reduced *fliC* expression in STM Δ*pflB* (**Figure S3B**). Additionally, 10
434 mM formate significantly upregulated *hilA*—the master regulator of SPI-1—in both strains
435 (**Figure S3C**).

436 The double knockout strain STM Δ*focAΔpflB* exhibited similar growth kinetics as STM WT in
437 LB broth and M9 Minimal Media (**Figure S4A, B**). However, due to its depleted formate pool,
438 it was also deficient in flagella, with partial recovery in anti-Fli MFI and adhesion in Caco-2

439 cell line when incubated with formate (**Figure S4 C, D, E**). In line with our previous findings,
440 we observed that oral gavaging of STM *ΔfocA* led to a similar bacterial burden in the liver and
441 the spleen as STM WT 5 dpi. STM *ΔfocAΔpflB* showed lesser organ burden in the liver and
442 spleen of the C57 mice model (**Figure S4 F**).

443

444

445 STM *ΔpflB* had a higher intracellular pH and higher membrane 446 depolarization, both of which were recovered upon F supplementation

447 Previous studies in *Escherichia coli* indicated that formate translocation through the FocA
448 channel and its metabolism via the FHL-1 (Formate Hydrogen Lyase-1) complex are crucial
449 for maintaining cellular pH homeostasis during anaerobic growth or fermentation [39-45]. This
450 raised the question of whether formate synthesis during aerobic growth in *Salmonella*
451 Typhimurium could also contribute to maintaining intracellular pH (ipH). Additionally, weak
452 acids like acetate and benzoate can cross the cell membrane in their neutral forms and
453 subsequently dissociate, thereby reducing ipH [46]. Based on this, we also hypothesized that
454 the endogenous formate pool might play a role in maintaining intracellular pH (ipH). To
455 investigate how changes in the surrounding media's pH affect intracellular pH, we incubated
456 STM WT and STM *ΔpflB* (+/- F) in phosphate buffers at pH levels 5.5, 6, and 7. After
457 incubation, we stained the cells with the pH-sensitive dye BCECF-AM. A higher 488/405 nm
458 fluorescence ratio for STM *ΔpflB* under all pH conditions indicated a higher ipH in the
459 knockout strain compared to the WT (**Figure 3A**).

460 To further confirm these results, we transformed STM WT and STM *ΔpflB* with the plasmid
461 pBAD-pHuji, which encodes a pH-sensitive red fluorescent protein. The higher ipH observed
462 in STM *ΔpflB*/pBAD-pHuji confirmed that *pflB* plays a significant role in maintaining

463 cytosolic pH in *Salmonella* Typhimurium. Consistent with the BCECF-AM staining results,
464 formate did not affect the ipH of STM WT/pBAD-pHuji (**Figure 3B**). These findings suggest
465 the possibility that extracellular and intracellular formate pools might independently regulate
466 the expression of *fliC* and *hilA* through distinct mechanisms.

467 One of the causes of membrane depolarization in biological systems is disrupted pH
468 homeostasis [47]. To investigate membrane potential in all strains with and without formate
469 supplementation, we analysed the exponential cultures of STM *ΔpflB* in LB. These cultures
470 showed a higher population of $DiBAC_4$-positive cells, indicating increased membrane
471 depolarization. Supplementation with formate successfully reduced membrane depolarization
472 in STM *ΔpflB*, but it had no effect on membrane polarization in STM WT (**Figure 3D, E**).
473 Similar results were observed when cells were stained with the DNA-binding fluorescent dye
474 bisbenzimide (**Figure 3C**).

475 Furthermore, the extent of membrane depolarization in STM *ΔpflB* was reduced when
476 stationary-phase bacteria were sub cultured into acidic F-media (pH 5) (**Figure 3E**). The H^+
477 ions in the acidic F-media may help counteract the disrupted cytosolic acidification in the *pflB*
478 knockout strain, thereby restoring membrane polarization.

479 These findings suggest that the intracellular formate pool is crucial for maintaining intracellular
480 pH (ipH) in *Salmonella* Typhimurium, which in turn supports cell membrane polarization. We
481 also explored whether the elevated ipH in the *pflB* knockout strain contributes to disrupted
482 flagellar apparatus synthesis. Incubation of STM *ΔpflB* in acidic LB medium (pH 6) led to an
483 increase in the *fliC* transcript level (**Figure S5 A**), indicating that higher ipH is responsible for
484 these downstream effects.

485

486

487 **STM *ΔpflB* had a higher transcript level of *csrB*, raising the possibility of**
488 **flagella inhibition via the *csr* sRNA system**

489 To investigate how formate regulates the flagellar operon, we measured the transcript levels of
490 several genes across different classes, including class I (*flhD*), class II (*flgA*,*fliA*), and class III
491 (*flgK*, *motA*) (**Figure 4A**) [48-56]. We discovered that in the formate-deficient *pflB* knockout
492 strain, inhibition of the flagellar operon begins at the level of class I genes or the genes that
493 regulate class I genes. The transcription of the *flhDC* promoter is controlled by various factors,
494 including OmpR, Crp, HdfR, H-NS, QseBC, FliA, LrhA, and others [50, 57-59]. One of the
495 most extensively studied mechanisms of post-transcriptional regulation of *flhDC* involves the
496 Csr system. The Csr system consists of the RNA-binding protein CsrA and the small regulatory
497 RNAs (sRNAs) *csrB* and *csrC* [60]. CsrA is a 61-amino-acid protein that binds to the mRNA
498 of target genes, thereby either inhibiting or enhancing their translation [61]. CsrA can bind to
499 the *flhD* transcript and stabilize it by preventing RNase E cleavage at the 5′ end [62]. The
500 activity of the CsrA protein is antagonized by small regulatory RNAs *csrB* and *csrC*. A single
501 *csrB* RNA molecule can bind up to 18 CsrA molecules, whereas a single *csrC* molecule can
502 bind up to 9 CsrA molecules [63-65]. In *S.* Typhimurium, CsrA has been seen to regulate
503 motility, virulence, carbon storage, and secondary metabolism [66, 67]. The transcription of
504 *csrB* and *csrC* is regulated by the BarA/SirA two-component systems (TCS) orthologues in *E.*
505 *coli* and *S.* Typhimurium[68-71].

506 We observed an increase in *csrB* transcript levels in STM *ΔpflB*, which decreased in STM
507 *ΔpflB*+F (**Figure 4B**). We also observed a reduction in *csrA* transcript levels in STM *ΔpflB,*
508 which was recovered upon incubation in F supplemented LB or LB with acidic pH (pH 6)
509 (**Figure S5B**). Since *csrB* directly binds to CsrA and inhibits its activity, we decided to clone
510 *csrA* into the extragenous plasmid pQE60 and transform this recombinant plasmid into STM

511 *ΔpflB*. Overexpressing *csrA* through IPTG induction partially restored the reduced expression
512 of *fliC* in STM *ΔpflB* (**Figure 4C**). CsrA is known to bind and stabilize the *flhD* transcript.
513 However, we speculate that an excess of CsrA molecules in the cell could potentially stabilize
514 *flhD* to the point of inhibiting its translation. This may explain why *csrA* overexpression in
515 STM WT led to a decrease in *fliC* expression. Overexpression of *csrA* mediated downregulation
516 of motility has been demonstrated in *Bacillus subtilis* and *Clostridium difficile* as well [72, 73].
517 The increase in flagellar numbers upon *csrA* overexpression in STM *ΔpflB* was visualized and
518 quantified using TEM and confocal microscopy (**Figure 4D**, **E, G**). This finding was
519 corroborated by an adhesion assay with the Caco-2 cell line, where STM *ΔpflB*/p: *csrA* showed
520 a higher adhesion percentage compared to STM *ΔpflB* (**Figure 4F**).

521

522 The extracytoplasmic sigma factor RpoE enhances the expression of csrB, 523 which in turn limits the expression of *fliC*

524 In *E. coli*, RpoE (σ^E) functions as an extracytoplasmic stress factor essential for cell viability
525 and regulating the response to membrane stress[74]. The membrane-bound anti-sigma factor
526 RseA binds to σ^E, aided by the periplasmic protein RseB [75, 76]. In the absence of envelope
527 stress, RseA binding inhibits σ^E from interacting with RNA polymerase [76-79]. When
528 envelope stress occurs, the proteolytically unstable RseA is quickly degraded, releasing free σ^E
529 molecules to carry out downstream functions. These functions include activating genes
530 involved in the biogenesis, transport, and assembly of lipopolysaccharides (LPS),
531 phospholipids, and outer membrane proteins (OMPs), as well as proteases and chaperones that
532 maintain or repair outer membrane (OM) integrity [76]. Recent studies have demonstrated that
533 σ^E also indirectly activates the transcription of *csrB*/*C* sRNAs from σ^{70} promoters [80, 81].
534 These findings have been established in *E. coli*. Deletion of *rpoE* in STM showed a reduction

535 in *csrB* transcript levels (~0.588), suggesting that a similar mechanism may operate in STM as
536 well **(Figure 5A)**.

537 Our previous data demonstrated that formate produced by PflB helps maintain the intracellular
538 pH (ipH) of the cell. Consequently, deletion of the *pflB* gene disrupts ipH balance, leading to
539 membrane depolarization. We hypothesized that this membrane stress in *STM ΔpflB* could
540 cause RseA degradation, thereby freeing σ^E to promote *csrB* transcription. Our results showed
541 that the elevated *csrB* expression observed in *STM ΔpflB* was significantly reduced in *STM*
542 *ΔpflBΔrpoE* (**Figure 5A**). Additionally, the suppressed expression of *flhD* and *fliC* in *STM*
543 *ΔpflB* was restored in *STM ΔpflBΔrpoE* (**Figure 5B**). Confocal microscopy and TEM provided
544 further confirmation of this finding (**Figure 5C-E**). However, we did not observe any recovery
545 in the swim halo upon deletion of *rpoE* from STM *ΔpflB*, which shows that the recovery in
546 translational level and protein level is not getting reflected in the motility of the attenuated
547 strain (**Figure 5F**). However, there was an improved adhesion of *STM ΔpflBΔrpoE* to Caco-2
548 cells compared to *STM ΔpflB* (**Figure 5G**). This improved adhesion might be due to the
549 enhanced hydrophobicity due to increased FliC protein in STM *ΔpflBΔrpoE* compared to STM
550 *ΔpflB* [38]. These results suggest that the reduction in flagella synthesis in STM *ΔpflB* could
551 be mediated by the extra cytoplasmic stress factor σ^E.

552

553 Formate regulates the balance between flagellar expression and SPI-1 gene
554 expression in the intestine of C57BL/6 mice

555 Our previous data showed that *STM ΔpflB* exhibited a higher abundance of the *prgH* transcript.
556 To determine if this increased expression of the SPI-1 gene was controlled by the same
557 regulatory loop, we analysed the transcript levels of the SPI-1 genes *hilA* and *prgH*. We found
558 that the elevated expression of *hilA* and *prgH* in *STM ΔpflB* was reduced in *STM ΔpflBΔrpoE*

559 (**Figure 6A**). This confirmed that intracellular formate regulates the shift from flagellar
560 expression to SPI-1 gene expression.

561 Our previous results showed that formate supplementation enhances *prgH* expression in both
562 STM WT and STM *ΔpflB* (**Figure 2A**). Flagellar motility and epithelial cell invasion are
563 regulated by the BarA/SirA two-component system (TCS) [70]. As expected, STM *ΔsirA*
564 exhibited low levels of *hilA* and *prgH* expression, and formate supplementation in STM *ΔsirA*
565 did not significantly alter the expression of these genes. Additionally, deletion of *sirA* in STM
566 *ΔpflB* eliminated any significant upregulation of *hilA* and *prgH* in response to formate
567 supplementation (**Figure 6B**). This indicates that extracellular formate influences the virulence
568 and pathogenicity of *Salmonella* via the BarA/SirA TCS.

569 Interestingly, we observed that STM *ΔpflBΔsirA* continued to show recovery in *fliC* transcript
570 levels under formate supplementation. This suggests that intracellular formate regulates
571 *Salmonella* pathogenesis independently of the BarA/SirA TCS (**Figure 6C**). Therefore, when
572 the intracellular formate pool is maintained by the *pflB* gene, extracellular formate modulates
573 SPI-1 gene expression through the BarA/SirA TCS. However, if the intracellular formate pool
574 is disrupted, the resulting membrane stress triggers RpoE-mediated overexpression of *csrB*,
575 which is associated with reduced *fliC* transcript levels and increased *hilA* and *prgH* expression.

576 As expected, STM *ΔsirA* exhibited low expression levels of *hilA* and *prgH*, and formate (F)
577 supplementation in STM *ΔsirA* did not result in any significant change in the expression of
578 these genes. Furthermore, deletion of *sirA* in STM *ΔpflB* eliminated any significant
579 upregulation of *hilA* and *prgH* in response to formate supplementation (**Figure 6B**). This
580 demonstrates that extracellular formate influences the virulence and pathogenesis of
581 *Salmonella* through the BarA/SirA TCS. Interestingly, we observed that STM *ΔpflBΔsirA*
582 continued to show recovery in *fliC* transcript levels with formate supplementation. This

583 indicates that intracellular formate regulates *Salmonella* pathogenesis independently of the
584 BarA/SirA TCS (**Figure 6C**). Thus, when the intracellular formate pool is maintained by the
585 *pflB* gene, extracellular formate modulates SPI-1 gene expression via the BarA/SirA TCS.
586 However, if the intracellular formate pool is disrupted, the resulting membrane stress triggers
587 RpoE-mediated overexpression of *csrB*, which is associated with reduced *fliC* transcript levels
588 and increased *hilA* and *prgH* expression. We proceeded to understand whether achieving
589 intracellular formate concentrations of STM *ΔpflB* to similar levels as STM WT and further
590 supplementing it with formate can replicate the behaviour of wild-type strain in presence of
591 formate. We subcultured the stationary phase cultures of STM WT and STM *ΔpflB* and
592 supplemented them higher concentrations of formate (70, 90, 110, 150 mM). We found that
593 there was a substantial decrease in the in the *fliC* transcript level in STM WT upon
594 supplementation of higher concentrations of formate. STM *ΔpflB* showed a remarkable
595 recovery in the *fliC* transcript level at 90 mM concentration, following which the expression
596 levels declined in the presence of 110 mM and 150 mM formate (**Figure 6D**). GC-MS mediated
597 quantification of intracellular formate concentration revealed that a concentration of 90 mM
598 was enough to replenish the depleted intracellular formate pool in STM *ΔpflB,* which explains
599 the highest expression of *fliC* at this concentration (**Figure 6E**). Beyond this, supplementation
600 of formate reduces the expression of *fliC* as seen in **Figure 6D**. This mimics the scenario of
601 supplementing F to STM WT with an intact formate pool. This was also visualized under TEM
602 and quantified by confocal microscopy (**Figure S6A, B, C**).

603 To explore the physiological relevance of this phenomenon, we examined *pflB* expression
604 levels in different sections of the intestine, since flagella and SPI-1 play critical roles in the
605 intestinal phase of *Salmonella* infection. We observed that *pflB* expression decreased
606 progressively from the duodenum to the ileum (**Figure 6F**). This finding led us to hypothesize
607 that *Salmonella* downregulates its *pflB* gene as it approaches its invasion site—the distal ileum.

608 This downregulation could induce a partial formate deficiency within the bacterial cell, causing
609 membrane depolarization, which in turn activates σ^E, increases *csrB* abundance, downregulates
610 flagellar operon transcription, and upregulates the SPI-1 gene cascade, ultimately help in
611 bacterial invasion at its target site of ileum.

612 To test this hypothesis, we collected duodenum and ileum sections from mice infected with
613 STM WT and STM *ΔpflB* and stained them with an anti-SipC antibody to measure levels of
614 the SPI-1 effector protein (**Figure 6G**). We normalized the fluorescence from the secondary
615 antibody, specific to the rabbit anti-SipC antibody, against mCherry fluorescence from bacteria
616 transformed with the pFPV plasmid. In mice infected with STM WT, we found that the
617 normalized mean fluorescence intensity (MFI) increased from the duodenum to the ileum. In
618 contrast, STM *ΔpflB*-infected mice showed a decrease in normalized MFI from the duodenum
619 to the ileum (**Figure 6H**). These results indicate that the formate pool maintained by the PflB
620 enzyme regulates SPI-1 gene expression, and its depletion may be a strategy used by
621 *Salmonella* Typhimurium to maximize SPI-1 expression, and thereby invasion, in the ileum.

622

623 # Discussion

624 *Salmonella* possesses a network of genes and regulatory factors that manages the balance
625 between its extracellular and intracellular modes of existence [82]. Research on *Salmonella*
626 Typhimurium has demonstrated overlapping regulatory mechanisms between the flagellar
627 secretion system and the SPI-1. The flagellar protein FliZ is known to activate the primary
628 regulator of flagella synthesis, FlhD, through post-translational modification. Kage *et al*. have
629 shown that FliZ can also regulate HilD, a key regulator of SPI-1, at the transcriptional level
630 [83, 84]. HilD has been found to bind directly to the promoter region of *flhDC*, upstream of the
631 P5 transcriptional start site, thus enhancing its expression [85]. Other studies indicate that SPI-

632 1 expression can suppress flagellar gene expression, aiding in pathogenicity and virulence of
633 *Salmonella*. A mutation in *fliZ* reduces *hilA* expression by half, while a knockout of *sirA*
634 decreases *hilA* expression tenfold and increases flagella expression a hundredfold [86-89].
635 Furthermore, recent research by Saleh *et al*. has shown that HilD activation can trigger a SPI-
636 1 dependent induction of the stringent response and significantly reduce the Proton Motive
637 Force (PMF). Although flagellation remains unaffected, HilD activation results in a motility
638 defect in *S.* Typhimurium [90]. Collectively, these studies reveal that *Salmonella* can toggle
639 between flagella synthesis and SPI-1 gene expression to optimize adhesion and the delivery of
640 SPI-1 effectors. There are several potential benefits to downregulating flagella while
641 upregulating SPI-1 genes. First, reducing flagella expression prevents the bacteria from moving
642 away from a target cell primed for invasion. Second, because the flagellar apparatus is
643 immunogenic, downregulating it may help the bacteria evade the host immune response [91-
644 93]. Lastly, simultaneous production of both systems could lead to interference, potentially
645 causing the improper secretion of flagellin and SPI-1 effectors [94].

646 In our study, we knocked out the gene encoding the pyruvate-formate lyase enzyme, effectively
647 depleting the cell of its native formate pool. Although the knockout strain displayed increased
648 expression of the SPI-1 gene *prgH*, it showed reduced transcript levels of *fliC*. This was
649 reflected in decreased invasion and adhesion capabilities in a human epithelial cell line. These
650 deficiencies were partially restored with the addition of 40 mM formate, which also explains
651 the strain's hyperproliferation in the RAW 264.7 macrophage cell line [95]. Additionally, we
652 found that the STM Δ*pflB* mutant was unable to maintain its intracellular pH to the same extent
653 as the STM wild type, resulting in a membrane depolarization phenotype. Membrane stress
654 triggered the sigma factor RpoE to increase the expression of *csrB*. Since *csrB* is known to bind
655 to and inhibit the CsrA protein, we hypothesized that the elevated *csrB* transcript levels led to
656 reduced *fliC* expression. Overexpressing *csrA* via an extragenous plasmid partially restored

657 *fliC* expression, supporting our hypothesis. Furthermore, deletion of *rpoE* in the STM Δ*pflB*
658 strain successfully reversed the flagella-deficient phenotype, providing further confirmation.
659 This demonstrated that the extra-cytoplasmic sigma factor RpoE mediates downstream effects
660 in response to cell membrane stress.

661 In all our experiments, we also observed that formate supplementation led to reduced flagellar
662 expression in STM WT. Interestingly, adding formate did not affect the intracellular pH or
663 membrane potential of STM WT, which led us to hypothesize that extracellular formate impacts
664 STM pathogenicity differently than intracellular formate synthesis. Huang *et al*. demonstrated
665 that extracellular formate functions as a diffusible signal to enhance invasion, but this effect
666 was independent of the BarA/SirA Two-Component System and was also unrelated to *csrB*,
667 which is directly regulated by the response regulator SirA. In our study, we found that STM
668 WT with formate supplementation (STM WT+F) showed higher expression of SPI-1 genes
669 [96]. Contrary to previous findings, we observed that *csrB* transcript levels were higher in STM
670 WT+F compared to STM WT, suggesting that elevated *csrB* levels might be linked to reduced
671 *fliC* expression [97]. This indicates that formate is a crucial metabolite for *Salmonella*, with a
672 critical concentration determining whether it acts through the TCS pathway or by regulating
673 the cell's intracellular pH. Additionally, we found that supplementing extracellular formate to
674 restore the intracellular formate pool caused STM Δ*pflB* to mimic the wild-type strain,
675 exhibiting reduced *fliC* levels in the presence of formate.

676 *Salmonella* Typhimurium has been extensively studied for its ability to adapt its metabolism to
677 conditions within the host. Previous research has shown that spatially distinct *Salmonella*
678 populations in the mucous layer and intestinal lumen differ in their energy metabolism.
679 Transcript levels of pyruvate-formate lyase and formate dehydrogenases were found to be
680 higher in the mucous layer than in the lumen population [16]. This formate metabolism
681 provided a fitness advantage in the mucous layer. In our study, we observed that *pflB*

682 transcription was highest in the large intestine and gradually decreased in the small intestine,
683 the primary site of *Salmonella* infection. This suggests that *Salmonella* modulates *pflB*
684 expression in response to local gut microenvironment signals. We propose a model in which
685 *Salmonella* downregulates the *pflB* gene upon reaching its infection site, disrupting its
686 intracellular formate pool. This can result in partial membrane depolarization, which
687 downregulates the flagellar apparatus and promotes invasion into epithelial cells through
688 upregulated expression of the SPI-1 system. The specific signals and genetic mechanisms
689 controlling this modulation remain unclear.

690 Overall, our study contributes to understanding how intracellular metabolism in *Salmonella*
691 influences its ability to adhere to and invade non-phagocytic intestinal epithelial cells, and it
692 highlights the potential for uncovering additional host-pathogen metabolic interactions in
693 future research.

694

695

696

697 # Acknowledgements

698 We acknowledge the Departmental Real-Time Facility, Departmental Confocal Microscopy
699 Facility, Divisional Electron Microscopy Facility, Divisional Mass Spectrometry Facility,
700 Divisional Flow Cytometry Facility, and Central Animal Facility at IISc for providing us
701 opportunity for experimentation. Mr. Sumitlal K and Ms. Navya have helped in image
702 acquisition in Confocal Microscopy. Dr. Sushma and Keerthana helped with image acquisition
703 in Transmission Electron Microscopy. Dr. Muralidhar and Dr. Sunitha helped in formate
704 quantitation studies using Gas Chromatography Mass Spectrometry. Ms. Lipika, Ms. Dharani,

and Mr. Munish helped in data acquisition from Flow Cytometry. Dr. Akshay Datey is acknowledged for his initial supervision in the study. The anti-SipC antibody was a kind gift from Prof. Dr. Ayub Qadri, National Institute of Immunology, Delhi, India.

Funding information

We express our heartfelt gratitude to the financial support from the Department of Biotechnology (DBT), Ministry of Science and Technology; Department of Science and Technology (DST), Ministry of Science and Technology. DC acknowledges DAE for the SRC Outstanding Investigator Award and funds, ASTRA Chair Professorship, and TATA Innovation fellowship funds. The authors jointly acknowledge the DBT-IISc Partnership Program. Infrastructure support from ICMR (Center for Advanced Study in Molecular Medicine), DST (FIST), and UGC-CAS (special assistance) is acknowledged. DM acknowledges the IISc fellowship. The funders had no role in study design, data collection and analysis, decision to publish, or preparation of the manuscript.

Author Contributions

DM and DC have conceived the study and designed the experiments. DM has performed all the experiments and participated in acquiring the data. DM has analysed the data, constructed the figures, and wrote the original draft of the manuscript. DM and DC have participated in the proofreading and editing of the manuscript. DC has supervised the study and helped in fund acquisition. All the authors have read and approved the manuscript.

Declaration of interest

The authors declare no conflict of interest.

Data availability

Data can be available from the authors upon reasonable request.

Data deposition

Link for pre-print: https://doi.org/10.1101/2024.01.30.577997

Thesis link

This research has not yet been included as part of any PhD thesis till current date.

References

1. Galanis, E., et al., *Web-based surveillance and global Salmonella distribution, 2000-2002.* Emerg Infect Dis, 2006. **12**(3): p. 381-8.
2. Collaborators, G.B.D.C.o.D., *Global, regional, and national age-sex-specific mortality for 282 causes of death in 195 countries and territories, 1980-2017: a systematic analysis for the Global Burden of Disease Study 2017.* Lancet, 2018. **392**(10159): p. 1736-1788.
3. DALYs, G.B.D. and H. Collaborators, *Global, regional, and national disability-adjusted life-years (DALYs) for 359 diseases and injuries and healthy life expectancy (HALE) for 195 countries and territories, 1990-2017: a systematic analysis for the Global Burden of Disease Study 2017.* Lancet, 2018. **392**(10159): p. 1859-1922.
4. Disease, G.B.D., I. Injury, and C. Prevalence, *Global, regional, and national incidence, prevalence, and years lived with disability for 354 diseases and injuries for 195 countries and territories, 1990-2017: a systematic analysis for the Global Burden of Disease Study 2017.* Lancet, 2018. **392**(10159): p. 1789-1858.

5. Crump, J.A., et al., *Epidemiology, Clinical Presentation, Laboratory Diagnosis, Antimicrobial Resistance, and Antimicrobial Management of Invasive Salmonella Infections.* Clin Microbiol Rev, 2015. **28**(4): p. 901-37.
6. Maslowski, K.M., et al., *Regulation of inflammatory responses by gut microbiota and chemoattractant receptor GPR43.* Nature, 2009. **461**(7268): p. 1282-6.
7. Tan, J., et al., *The role of short-chain fatty acids in health and disease.* Advances in immunology, 2014. **121**: p. 91-119.
8. Thorburn, A.N., L. Macia, and C.R. Mackay, *Diet, metabolites, and "western-lifestyle" inflammatory diseases.* Immunity, 2014. **40**(6): p. 833-42.
9. Huffnagle, G.B., *Increase in dietary fiber dampens allergic responses in the lung.* Nat Med, 2014. **20**(2): p. 120-1.
10. Machado, M.G., V. Sencio, and F. Trottein, *Short-Chain Fatty Acids as a Potential Treatment for Infections: a Closer Look at the Lungs.* Infect Immun, 2021. **89**(9): p. e0018821.
11. Boyen, F., et al., *Coated fatty acids alter virulence properties of Salmonella Typhimurium and decrease intestinal colonization of pigs.* Veterinary microbiology, 2008. **132**(3-4): p. 319-327.
12. Gantois, I., et al., *Butyrate specifically down-regulates Salmonella pathogenicity island 1 gene expression.* Applied and environmental microbiology, 2006. **72**(1): p. 946-949.
13. Lawhon, S.D., et al., *Intestinal short-chain fatty acids alter Salmonella typhimurium invasion gene expression and virulence through BarA/SirA.* Molecular microbiology, 2002. **46**(5): p. 1451-1464.
14. Chowdhury, R., et al., *Salmonella Invasion Is Controlled by Competition among Intestinal Chemical Signals.* mBio, 2023. **14**(2): p. e0001223.
15. Chowdhury, R., et al., *Salmonella Invasion Is Controlled by Competition among Intestinal Chemical Signals.* mBio, 2023. **14**(2): p. e00012-23.
16. Winter, M.G., et al., *Formate oxidation in the intestinal mucus layer enhances fitness of Salmonella enterica serovar Typhimurium.* mBio, 2023. **14**(4): p. e0092123.
17. Huang, Y., et al., *Formate Acts as a Diffusible Signal To Induce Salmonella Invasion.* Journal of Bacteriology, 2008. **190**(12): p. 4233-4241.
18. Winter, M.G., et al., *Formate oxidation in the intestinal mucus layer enhances fitness of Salmonella enterica serovar Typhimurium.* Mbio, 2023. **14**(4): p. e00921-23.
19. Abernathy, J., et al., *Deletions in the pyruvate pathway of Salmonella Typhimurium alter SPI1-mediated gene expression and infectivity.* J Anim Sci Biotechnol, 2013. **4**(1): p. 5.
20. Datsenko, K.A. and B.L. Wanner, *One-step inactivation of chromosomal genes in Escherichia coli K-12 using PCR products.* Proc Natl Acad Sci U S A, 2000. **97**(12): p. 6640-5.
21. Gagnon, M., et al., *Comparison of the Caco-2, HT-29 and the mucus-secreting HT29-MTX intestinal cell models to investigate Salmonella adhesion and invasion.* J Microbiol Methods, 2013. **94**(3): p. 274-9.
22. Marathe, S.A., et al., *Curcumin Reduces the Motility of Salmonella enterica Serovar Typhimurium by Binding to the Flagella, Thereby Leading to Flagellar Fragility and Shedding.* J Bacteriol, 2016. **198**(13): p. 1798-1811.
23. Hughes, E.R., et al., *Microbial Respiration and Formate Oxidation as Metabolic Signatures of Inflammation-Associated Dysbiosis.* Cell Host Microbe, 2017. **21**(2): p. 208-219.
24. Roy Chowdhury, A., et al., *Salmonella Typhimurium outer membrane protein A (OmpA) renders protection from nitrosative stress of macrophages by maintaining the stability of bacterial outer membrane.* PLoS Pathog, 2022. **18**(8): p. e1010708.
25. Chowdhury, A.R., et al., *Loss of outer membrane protein A (OmpA) impairs the survival of Salmonella Typhimurium by inducing membrane damage in the presence of ceftazidime and meropenem.* J Antimicrob Chemother, 2022. **77**(12): p. 3376-3389.
26. Shen, Y., et al., *pHuji, a pH-sensitive red fluorescent protein for imaging of exo- and endocytosis.* J Cell Biol, 2014. **207**(3): p. 419-32.

27. Hajra, D., et al., *SIRT1 and SIRT3 impact host mitochondrial function and host-Salmonella pH balance during infection.* bioRxiv, 2023: p. 2023.09.11.557159.
28. Chandra, K., et al., *GH18 family glycoside hydrolase Chitinase A of Salmonella enhances virulence by facilitating invasion and modulating host immune responses.* PLoS Pathog, 2022. **18**(4): p. e1010407.
29. Lu, W., et al., *pH-dependent gating in a FocA formate channel.* Science, 2011. **332**(6027): p. 352-4.
30. Dong, R., et al., *DsrA Modulates Central Carbon Metabolism and Redox Balance by Directly Repressing pflB Expression in Salmonella Typhimurium.* Microbiol Spectr, 2022. **10**(1): p. e0152221.
31. Parker, C.T. and J. Guard-Petter, *Contribution of flagella and invasion proteins to pathogenesis of Salmonella enterica serovar enteritidis in chicks.* FEMS microbiology letters, 2001. **204**(2): p. 287-291.
32. Haiko, J. and B. Westerlund-Wikstrom, *The role of the bacterial flagellum in adhesion and virulence.* Biology (Basel), 2013. **2**(4): p. 1242-67.
33. Rossez, Y., et al., *Bacterial flagella: twist and stick, or dodge across the kingdoms.* PLoS Pathog, 2015. **11**(1): p. e1004483.
34. Gut, A.M., et al., *Salmonella infection - prevention and treatment by antibiotics and probiotic yeasts: a review.* Microbiology (Reading), 2018. **164**(11): p. 1327-1344.
35. Agbor, T.A. and B.A. McCormick, *Salmonella effectors: important players modulating host cell function during infection.* Cell Microbiol, 2011. **13**(12): p. 1858-69.
36. Finlay, B.B., S. Ruschkowski, and S. Dedhar, *Cytoskeletal rearrangements accompanying salmonella entry into epithelial cells.* J Cell Sci, 1991. **99 (Pt 2)**: p. 283-96.
37. Zhou, D. and J. Galan, *Salmonella entry into host cells: the work in concert of type III secreted effector proteins.* Microbes Infect, 2001. **3**(14-15): p. 1293-8.
38. Horstmann, J.A., et al., *Methylation of Salmonella Typhimurium flagella promotes bacterial adhesion and host cell invasion.* Nature communications, 2020. **11**(1): p. 2013.
39. Kammel, M., C. Pinske, and R.G. Sawers, *FocA and its central role in fine-tuning pH homeostasis of enterobacterial formate metabolism.* Microbiology (Reading), 2022. **168**(10).
40. Suppmann, B. and G. Sawers, *Isolation and characterization of hypophosphite-resistant mutants of Escherichia coli: identification of the FocA protein, encoded by the pfl operon, as a putative formate transporter.* Molecular Microbiology, 1994. **11**(5): p. 965-982.
41. Kammel, M. and R.G. Sawers, *The FocA channel functions to maintain intracellular formate homeostasis during Escherichia coli fermentation.* Microbiology, 2022. **168**(4).
42. Beyer, L., et al., *Coordination of FocA and pyruvate formate-lyase synthesis in Escherichia coli demonstrates preferential translocation of formate over other mixed-acid fermentation products.* J Bacteriol, 2013. **195**(7): p. 1428-35.
43. Wiechert, M. and E. Beitz, *Mechanism of formate-nitrite transporters by dielectric shift of substrate acidity.* EMBO J, 2017. **36**(7): p. 949-958.
44. Lyu, M., et al., *Structural basis of transport and inhibition of the Plasmodium falciparum transporter PfFNT.* EMBO reports, 2021. **22**(3): p. e51628.
45. Helmstetter, F., et al., *Formate-nitrite transporters carrying nonprotonatable amide amino acids instead of a central histidine maintain pH-dependent transport.* J Biol Chem, 2019. **294**(2): p. 623-631.
46. Minamino, T., et al., *Effect of intracellular pH on rotational speed of bacterial flagellar motors.* J Bacteriol, 2003. **185**(4): p. 1190-4.
47. Putnam, R.W., *Chapter 17 - Intracellular pH Regulation*, in *Cell Physiology Source Book (Fourth Edition)*, N. Sperelakis, Editor. 2012, Academic Press: San Diego. p. 303-321.
48. Kutsukake, K. and N. Ide, *Transcriptional analysis of the flgK and fliD operons of Salmonella typhimurium which encode flagellar hook-associated proteins.* Mol Gen Genet, 1995. **247**(3): p. 275-81.

855 49. Gillen, K.L. and K.T. Hughes, *Transcription from two promoters and autoregulation contribute*
856 *to the control of expression of the Salmonella typhimurium flagellar regulatory gene flgM.* J
857 Bacteriol, 1993. **175**(21): p. 7006-15.
858 50. Ikebe, T., S. Iyoda, and K. Kutsukake, *Structure and expression of the fliA operon of Salmonella*
859 *typhimurium.* Microbiology (Reading), 1999. **145 (Pt 6)**: p. 1389-1396.
860 51. Ohnishi, K., et al., *Gene fliA encodes an alternative sigma factor specific for flagellar operons*
861 *in Salmonella typhimurium.* Mol Gen Genet, 1990. **221**(2): p. 139-47.
862 52. Karlinsey, J.E., et al., *Completion of the hook-basal body complex of the Salmonella*
863 *typhimurium flagellum is coupled to FlgM secretion and fliC transcription.* Mol Microbiol,
864 2000. **37**(5): p. 1220-31.
865 53. Ohnishi, K., et al., *A novel transcriptional regulation mechanism in the flagellar regulon of*
866 *Salmonella typhimurium: an antisigma factor inhibits the activity of the flagellum-specific*
867 *sigma factor, sigma F.* Mol Microbiol, 1992. **6**(21): p. 3149-57.
868 54. Fraser, G.M., et al., *Substrate specificity of type III flagellar protein export in Salmonella is*
869 *controlled by subdomain interactions in FlhB.* Mol Microbiol, 2003. **48**(4): p. 1043-57.
870 55. Hirano, T., et al., *Substrate specificity classes and the recognition signal for Salmonella type III*
871 *flagellar export.* J Bacteriol, 2003. **185**(8): p. 2485-92.
872 56. Frye, J., et al., *Identification of new flagellar genes of Salmonella enterica serovar*
873 *Typhimurium.* J Bacteriol, 2006. **188**(6): p. 2233-43.
874 57. Kutsukake, K., *Autogenous and global control of the flagellar master operon, flhD, in*
875 *Salmonella typhimurium.* Mol Gen Genet, 1997. **254**(4): p. 440-8.
876 58. Tanabe, Y., et al., *The transcript from the sigma(28)-dependent promoter is translationally*
877 *inert in the expression of the sigma(28)-encoding gene fliA in the fliAZ operon of Salmonella*
878 *enterica serovar Typhimurium.* J Bacteriol, 2011. **193**(22): p. 6132-41.
879 59. Ko, M. and C. Park, *H-NS-Dependent regulation of flagellar synthesis is mediated by a LysR*
880 *family protein.* J Bacteriol, 2000. **182**(16): p. 4670-2.
881 60. Vakulskas, C.A., et al., *Regulation of bacterial virulence by Csr (Rsm) systems.* Microbiol Mol
882 Biol Rev, 2015. **79**(2): p. 193-224.
883 61. Romeo, T., *Global regulation by the small RNA-binding protein CsrA and the non-coding RNA*
884 *molecule CsrB.* Mol Microbiol, 1998. **29**(6): p. 1321-30.
885 62. Yakhnin, A.V., et al., *CsrA activates flhDC expression by protecting flhDC mRNA from RNase E-*
886 *mediated cleavage.* Mol Microbiol, 2013. **87**(4): p. 851-66.
887 63. Liu, M.Y., et al., *The RNA molecule CsrB binds to the global regulatory protein CsrA and*
888 *antagonizes its activity in Escherichia coli.* J Biol Chem, 1997. **272**(28): p. 17502-10.
889 64. Weilbacher, T., et al., *A novel sRNA component of the carbon storage regulatory system of*
890 *Escherichia coli.* Mol Microbiol, 2003. **48**(3): p. 657-70.
891 65. Dubey, A.K., et al., *RNA sequence and secondary structure participate in high-affinity CsrA-*
892 *RNA interaction.* RNA, 2005. **11**(10): p. 1579-87.
893 66. Altier, C., M. Suyemoto, and S.D. Lawhon, *Regulation of Salmonella enterica serovar*
894 *typhimurium invasion genes by csrA.* Infect Immun, 2000. **68**(12): p. 6790-7.
895 67. Lawhon, S.D., et al., *Global regulation by CsrA in Salmonella typhimurium.* Mol Microbiol,
896 2003. **48**(6): p. 1633-45.
897 68. Suzuki, K., et al., *Regulatory circuitry of the CsrA/CsrB and BarA/UvrY systems of Escherichia*
898 *coli.* J Bacteriol, 2002. **184**(18): p. 5130-40.
899 69. Suzuki, K., et al., *Regulatory circuitry of the CsrA/CsrB and BarA/UvrY systems of Escherichia*
900 *coli.* Journal of bacteriology, 2002. **184**(18): p. 5130-5140.
901 70. Teplitski, M., R.I. Goodier, and B.M. Ahmer, *Pathways Leading from BarA/SirA to Motility*
902 *andVirulence Gene Expression in Salmonella.* Journal of bacteriology, 2003. **185**(24): p. 7257-
903 7265.
904 71. Weilbacher, T., et al., *A novel sRNA component of the carbon storage regulatory system of*
905 *Escherichia coli.* Molecular microbiology, 2003. **48**(3): p. 657-670.

72. Gu, H., et al., *Carbon storage regulator CsrA plays important roles in multiple virulence-associated processes of Clostridium difficile.* Microbial pathogenesis, 2018. **121**: p. 303-309.
73. Yakhnin, H., et al., *CsrA of Bacillus subtilis regulates translation initiation of the gene encoding the flagellin protein (hag) by blocking ribosome binding.* Molecular microbiology, 2007. **64**(6): p. 1605-1620.
74. Hayden, J.D. and S.E. Ades, *The extracytoplasmic stress factor, sigmaE, is required to maintain cell envelope integrity in Escherichia coli.* PLoS One, 2008. **3**(2): p. e1573.
75. Ahuja, N., et al., *Analyzing the interaction of RseA and RseB, the two negative regulators of the sigmaE envelope stress response, using a combined bioinformatic and experimental strategy.* J Biol Chem, 2009. **284**(8): p. 5403-13.
76. Lima, S., et al., *Dual molecular signals mediate the bacterial response to outer-membrane stress.* Science, 2013. **340**(6134): p. 837-41.
77. De Las Penas, A., L. Connolly, and C.A. Gross, *The sigmaE-mediated response to extracytoplasmic stress in Escherichia coli is transduced by RseA and RseB, two negative regulators of sigmaE.* Mol Microbiol, 1997. **24**(2): p. 373-85.
78. Missiakas, D., et al., *Modulation of the Escherichia coli sigmaE (RpoE) heat-shock transcription-factor activity by the RseA, RseB and RseC proteins.* Mol Microbiol, 1997. **24**(2): p. 355-71.
79. Campbell, E.A., et al., *Crystal structure of Escherichia coli sigmaE with the cytoplasmic domain of its anti-sigma RseA.* Mol Cell, 2003. **11**(4): p. 1067-78.
80. Pannuri, A., et al., *Circuitry Linking the Catabolite Repression and Csr Global Regulatory Systems of Escherichia coli.* J Bacteriol, 2016. **198**(21): p. 3000-3015.
81. Yakhnin, H., et al., *Circuitry Linking the Global Csr- and sigma(E)-Dependent Cell Envelope Stress Response Systems.* J Bacteriol, 2017. **199**(23).
82. Fabrega, A. and J. Vila, *Salmonella enterica serovar Typhimurium skills to succeed in the host: virulence and regulation.* Clin Microbiol Rev, 2013. **26**(2): p. 308-41.
83. Kage, H., et al., *Coordinated regulation of expression of Salmonella pathogenicity island 1 and flagellar type III secretion systems by ATP-dependent ClpXP protease.* J Bacteriol, 2008. **190**(7): p. 2470-8.
84. Saini, S., et al., *FliZ Is a posttranslational activator of FlhD4C2-dependent flagellar gene expression.* J Bacteriol, 2008. **190**(14): p. 4979-88.
85. Singer, H.M., et al., *The Salmonella Spi1 virulence regulatory protein HilD directly activates transcription of the flagellar master operon flhDC.* J Bacteriol, 2014. **196**(7): p. 1448-57.
86. Eichelberg, K. and J.E. Galan, *The flagellar sigma factor FliA (sigma(28)) regulates the expression of Salmonella genes associated with the centisome 63 type III secretion system.* Infect Immun, 2000. **68**(5): p. 2735-43.
87. Iyoda, S., et al., *A flagellar gene fliZ regulates the expression of invasion genes and virulence phenotype in Salmonella enterica serovar Typhimurium.* Microb Pathog, 2001. **30**(2): p. 81-90.
88. Lucas, R.L., et al., *Multiple factors independently regulate hilA and invasion gene expression in Salmonella enterica serovar typhimurium.* J Bacteriol, 2000. **182**(7): p. 1872-82.
89. Goodier, R.I. and B.M. Ahmer, *SirA orthologs affect both motility and virulence.* J Bacteriol, 2001. **183**(7): p. 2249-58.
90. Saleh, D.O., et al., *SPI-1 virulence gene expression modulates motility of Salmonella Typhimurium in a proton motive force- and adhesins-dependent manner.* PLoS Pathog, 2023. **19**(6): p. e1011451.
91. Gewirtz, A.T., et al., *Salmonella typhimurium induces epithelial IL-8 expression via Ca(2+)-mediated activation of the NF-kappaB pathway.* J Clin Invest, 2000. **105**(1): p. 79-92.
92. McSorley, S.J., B.T. Cookson, and M.K. Jenkins, *Characterization of CD4+ T cell responses during natural infection with Salmonella typhimurium.* J Immunol, 2000. **164**(2): p. 986-93.

93. Takahashi, A., et al., *Production of beta-defensin-2 by human colonic epithelial cells induced by Salmonella enteritidis flagella filament structural protein.* FEBS Lett, 2001. **508**(3): p. 484-8.
94. Ellermeier, C.D. and J.M. Slauch, *RtsA and RtsB coordinately regulate expression of the invasion and flagellar genes in Salmonella enterica serovar Typhimurium.* J Bacteriol, 2003. **185**(17): p. 5096-108.
95. Olsen, J.E., et al., *The role of flagella and chemotaxis genes in host pathogen interaction of the host adapted Salmonella enterica serovar Dublin compared to the broad host range serovar S. Typhimurium.* BMC Microbiol, 2013. **13**: p. 67.
96. Huang, Y., et al., *Formate acts as a diffusible signal to induce Salmonella invasion.* J Bacteriol, 2008. **190**(12): p. 4233-41.
97. Teplitski, M., R.I. Goodier, and B.M. Ahmer, *Pathways leading from BarA/SirA to motility and virulence gene expression in Salmonella.* J Bacteriol, 2003. **185**(24): p. 7257-65.

Tables:

Table 1: List of strains

Strains/ plasmids	**Characteristics**	**Source/ Information**
Salmonella enterica subspecies *enterica* serovar Typhimurium strain 14028S	Wild type (WT)	Gift from Prof. M. Hensel
S. Typhimurium *ΔfocA*	Chl^R	This study
S. Typhimurium *ΔpflB*	Kan^R	This study
S. Typhimurium *ΔpflB*/pQE60	Kan^R, Amp^R	This study
S. Typhimurium *ΔpflB*/pQE60: *pflB*	Kan^R, Amp^R	This study
S. Typhimurium *ΔfocAΔpflB*	Kan^R, Chl^R	This study
S. Typhimurium *ΔfliC*	Kan^R	Laboratory stock
S. Typhimurium/pQE60: *csrA*	Amp^R	This study
S. Typhimurium *ΔpflB*/pQE60: *csrA*	Kan^R, Amp^R	This study

pKD4	Plasmid with FRT flanked Kanamycin-resistant cassette	
pKD3	Plasmid with FRT flanked Chloramphenicol-resistant cassette	
pKD46	Plasmid expressing λ-red recombinase system, Amp^R	
pQE60 vector	Low copy number plasmid, Amp^R	Laboratory stock
pHuji		Addgene

972

973

974

975

976

977

978

979

980

981

982 **Table 2: List of primers:**

PRIMER NAME	SEQUENCE (5'-3')
16S rRNA RT FP	GTGAGGTAACGGCTCACCAA
16S rRNA RT RP	TAACCGCAACACCTTCCTCC
hilA RT FP	GCCGGTGACCATTACGAAGA
hilA RT RP	AAGAGAGAAGCGGGTTGGTG
prgH RT FP	CGTTTTCAGGTGTTGCCAGG
prgH RT RP	TACGCGGCTCATCGAAATGA
flhD RT FP	CGCCTCGGTATCAACGAAGA
flhD RT RP	CACTTCATTGAGCAGACGCG
fliC RT FP	CTAAACAAACTGGGTGGCGC

fliC RT RP	GCACCCAGGTCAGAACGTAA
flgA RT FP	ATTATGTCGCCGTTGCC
flgA RT RP	TGACCTGTACTCGTTGC
flgK RT FP	AACCACCGATCAGTATC
flgK RT RP	TCGTCAGGTTATAGGTG
fliA RT FP	GCTGGATGAATTACGCA
fliA RT RP	CCACTCATCGTAAGAGA
motA RT FP	TTGCTGGCGTTGCTCTA
motA RT RP	GATGATCAGGCGCAGAT
csrB RT FP	CGTACAACGAAGCGAACGTC
csrB RT RP	TGTGACCTTACGGCCTGTTC
focA KO FP	ACACCGTAATTGCATAAAAGCCATGCGACTTACGGGCCTACATATGAAT ATCCTCCTTAG

focA KO RP	ATGCTCGTTACCACGCAGGTAAATGACCCAGTATGTCAACGTGTAGGCTGGAGCTGCTTC
pflB KO FP	ATGTCCGAGCTTAATGAAAAGTTAGCCACAGCCTGGGAACATATGAATATCCTCCTTAG
pflB KO RP	TACATGGTCTGCGTGAAGGTACGAGTAATAACGTCCTGCTGTGTAGGCTGGAGCTGCTTC
focA RT FP	CGGAAAGCCACATCAGTAAC
focA RT RP	ATCGGGGGTATCTGTTTCTC
pflB RT FP	ATAACGTCCTGCTGCTGTTC
pflB RT RP	ATGGTTACTTCCACCACGAA
pflB cloning FP	CGCGGATCCATGTCCGAGCTTAATGA
pflB cloning RP	CCCAAGCTTCAGTCAAACCCATTACA
rpoE KO FP	GGTTTGGGGAGACATTACCTCGGATGAGCGAGCAGTTACATATGAATATCCTCCTTAG
rpoE KO RP	CCTAATACCTTTTCCAGTATCCCGCTATCGTCAACGGTGTAGGCTGGAGCTGCTTC

sirA KO FP	CTATCAGTAGCGTTATCCCTATTCTGGAGATATTCCTTTGCATATGAATATCCTCCTTAG
sirA KO RP	ATACGATAGCGATAGCTGTTCACCGTTTTAGGACTGAGATGTGTAGGCTGGAGCTCTTC
csrA cloning FP	CGCGGATCCATGCTGATTCTGACTCG
csrA cloning RP	CCCAAGCTTTTAGTAACTGGACTGCTGG

983

984 # Figures

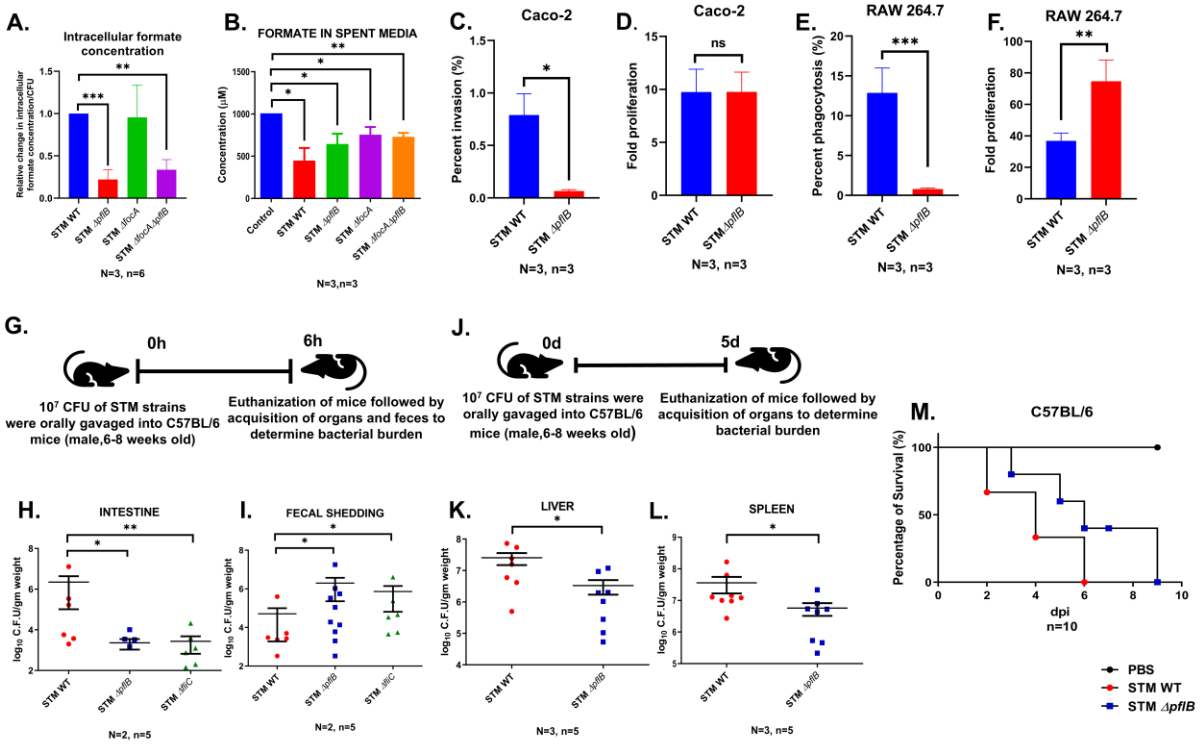
A.
Intracellular formate concentration
Relative change in intracellular formate concentration/CFU
STM WT
STM ΔpflB
STM ΔfocA
STM ΔfocA,pflB
N=3, n=6
B.
FORMATE IN SPENT MEDIA
Concentration (μM)
Control
STM WT
STM ΔpflB
STM ΔfocA
STM ΔfocA,pflB
N=3,n=3
C.
Caco-2
Percent invasion (%)
STM WT
STM ΔpflB
N=3, n=3
D.
Caco-2
ns
Fold proliferation
STM WT
STM ΔpflB
N=3, n=3
E.
RAW 264.7
Percent phagocytosis (%)
STM WT
STM ΔpflB
N=3, n=3
F.
RAW 264.7
Fold proliferation
STM WT
STM ΔpflB
N=3, n=3
G.
0h
6h
10⁷ CFU of STM strains were orally gavaged into C57BL/6 mice (male,6-8 weeks old)
Euthanization of mice followed by acquisition of organs and feces to determine bacterial burden
J.
0d
5d
10⁷ CFU of STM strains were orally gavaged into C57BL/6 mice (male,6-8 weeks old)
Euthanization of mice followed by acquisition of organs to determine bacterial burden
M.
C57BL/6
Percentage of Survival (%)
dpi
n=10
PBS
STM WT
STM ΔpflB
H.
INTESTINE
log10 C.F.U/gm weight
STM WT
STM ΔpflB
STM ΔfliC
N=2, n=5
I.
FECAL SHEDDING
log10 C.F.U/gm weight
STM WT
STM ΔpflB
STM ΔfliC
N=2, n=5
K.
LIVER
log10 C.F.U/gm weight
STM WT
STM ΔpflB
N=3, n=5
L.
SPLEEN
log10 C.F.U/gm weight
STM WT
STM ΔpflB
N=3, n=5

Figure 1

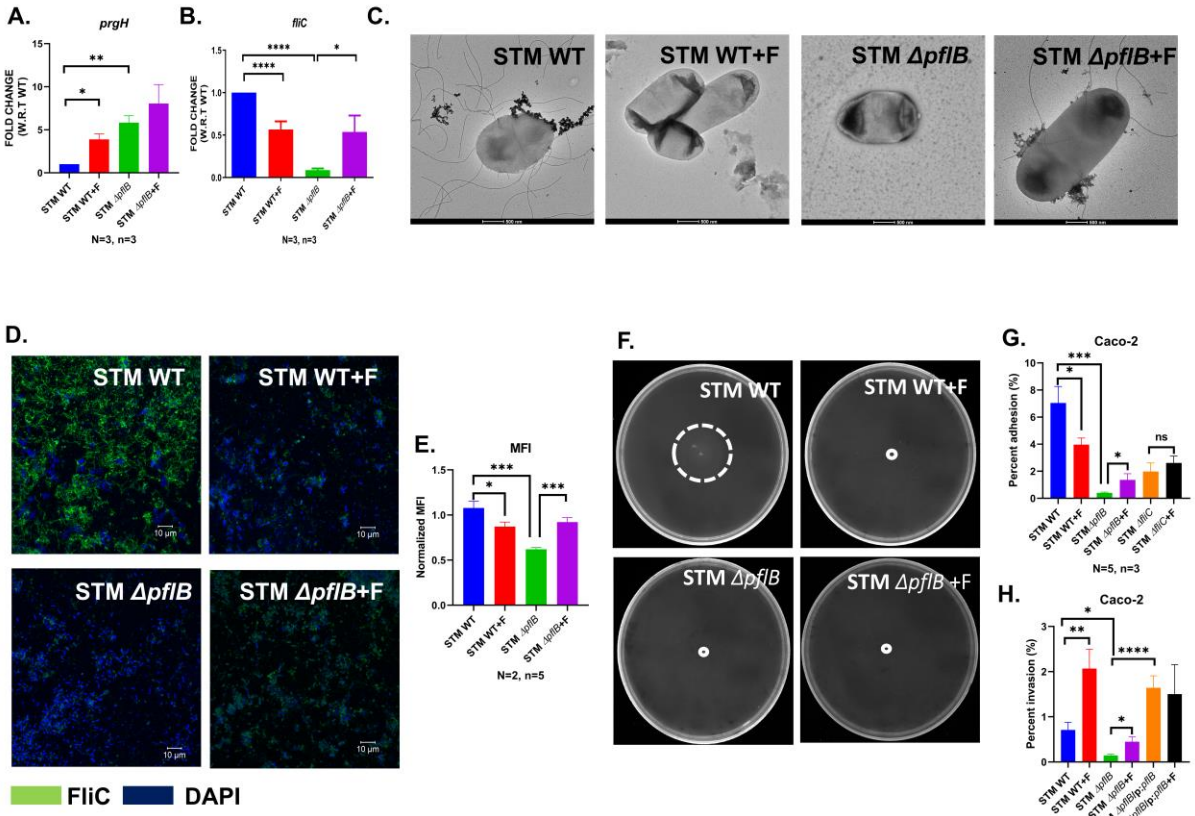
A.
prgH
FOLD CHANGE (W.R.T WT)
STM WT
STM WT+F
STM ΔpflB
STM ΔpflB+F
N=3, n=3
B.
fliC
FOLD CHANGE (W.R.T WT)
N=3, n=3
C.
STM WT
STM WT+F
STM ΔpflB
STM ΔpflB+F
D.
STM WT
STM WT+F
STM ΔpflB
STM ΔpflB+F
10 µm
FliC
DAPI
E.
MFI
Normalized MFI
N=2, n=5
F.
STM WT
STM WT+F
STM ΔpflB
STM ΔpflB +F
G.
Caco-2
Percent adhesion (%)
ns
STM ΔfliC
STM ΔfliC+F
N=5, n=3
H.
Caco-2
Percent invasion (%)
STM ΔpflB:pflB
STM ΔpflB:pflB+F
N=2,n=2

986 **Figure 2**

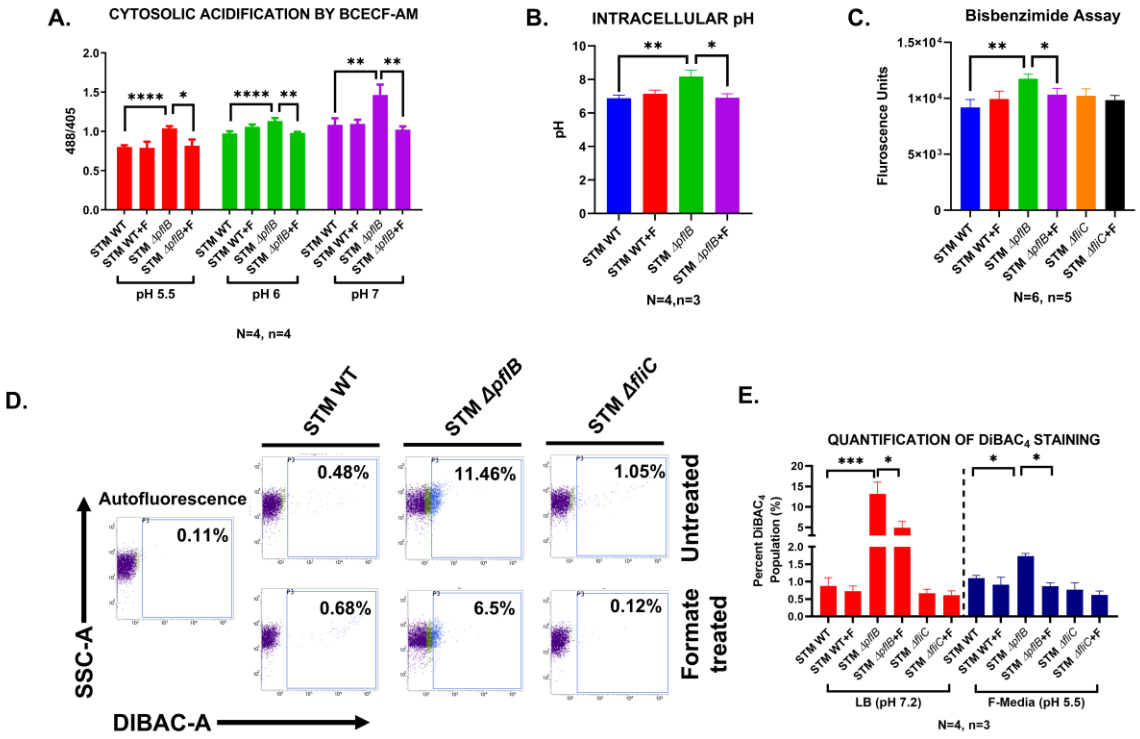
A.
CYTOSOLIC ACIDIFICATION BY BCECF-AM
488/405
STM WT
STM WT+F
STM ΔpflB
STM ΔpflB+F
pH 5.5
pH 6
pH 7
N=4, n=4
B.
INTRACELLULAR pH
pH
N=4,n=3
C.
Bisbenzimide Assay
Fluroscence Units
STM ΔfliC
STM ΔfliC+F
N=6, n=5
D.
STM WT
STM ΔpflB
STM ΔfliC
Autofluorescence
0.11%
0.48%
11.46%
1.05%
0.68%
6.5%
0.12%
Untreated
Formate treated
SSC-A
DIBAC-A
E.
QUANTIFICATION OF DiBAC4 STAINING
Percent DiBAC4 Population (%)
LB (pH 7.2)
F-Media (pH 5.5)
N=4, n=3

Figure 3

987

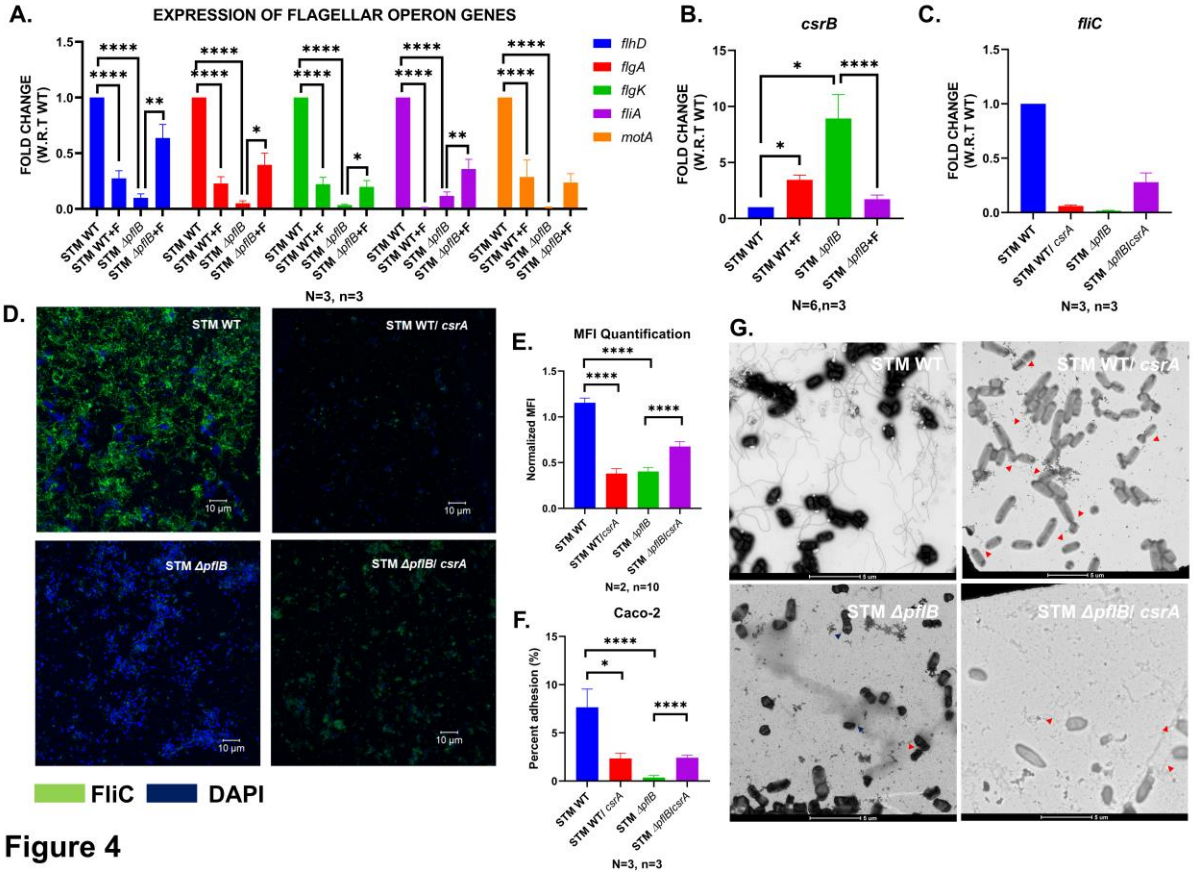

Figure 4

988

989

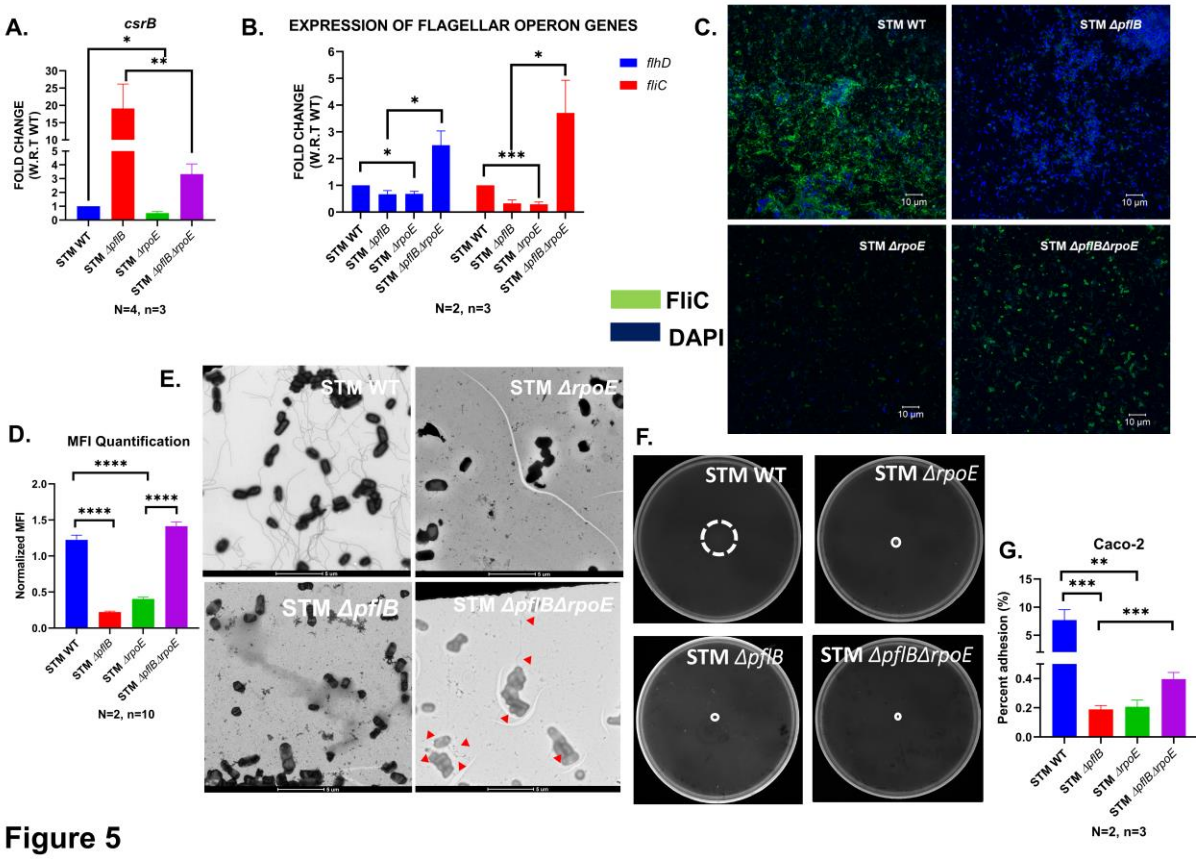
A.
csrB
FOLD CHANGE (W.R.T WT)
STM WT
STM ΔpflB
STM ΔrpoE
STM ΔpflBΔrpoE
N=4, n=3
B.
EXPRESSION OF FLAGELLAR OPERON GENES
flhD
fliC
N=2, n=3
C.
STM WT
STM ΔpflB
STM ΔrpoE
STM ΔpflBΔrpoE
FliC
DAPI
D.
MFI Quantification
Normalized MFI
N=2, n=10
E.
F.
G.
Caco-2
Percent adhesion (%)
N=2, n=3

Figure 5

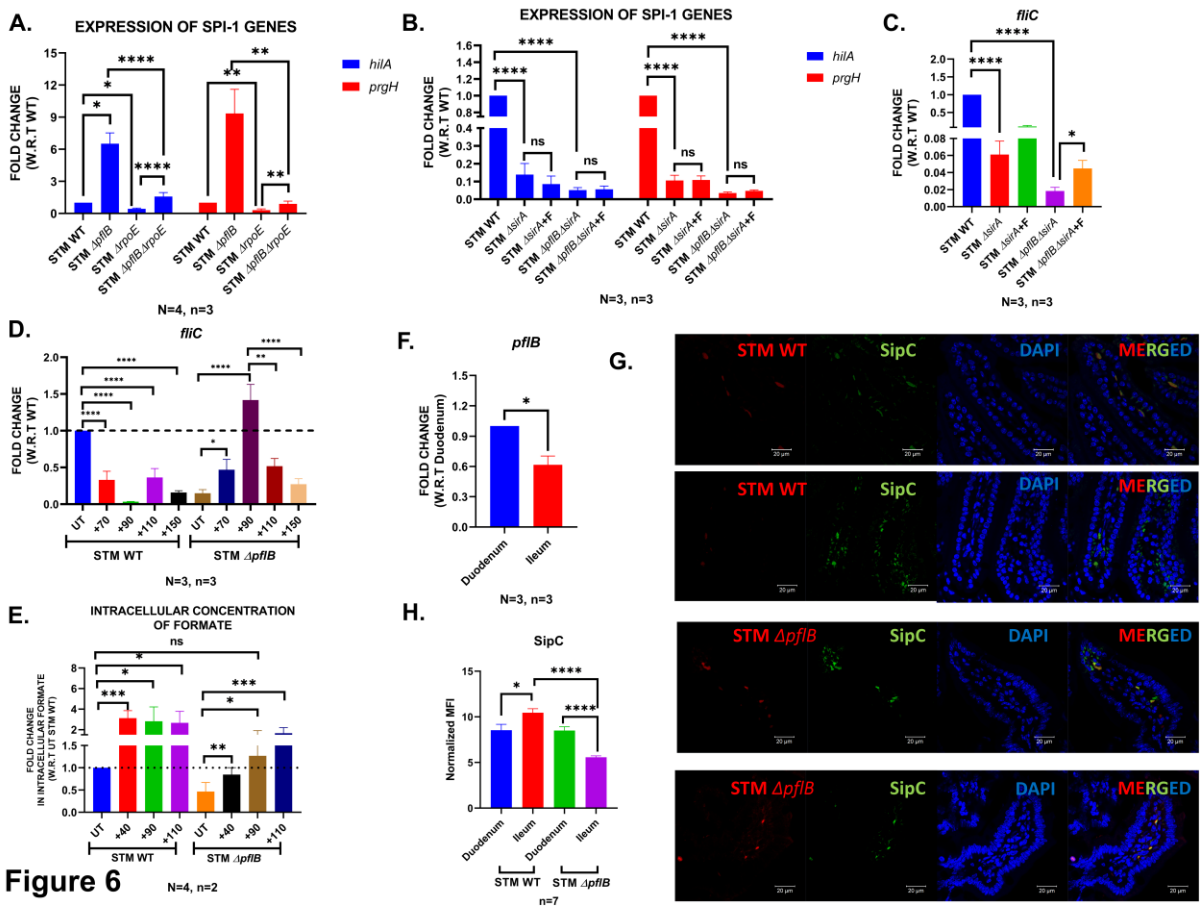
A.
EXPRESSION OF SPI-1 GENES
FOLD CHANGE (W.R.T WT)
hilA
prgH
STM WT
STM ΔpflB
STM ΔrpoE
STM ΔpflBΔrpoE
N=4, n=3
B.
EXPRESSION OF SPI-1 GENES
FOLD CHANGE (W.R.T WT)
hilA
prgH
STM WT
STM ΔsirA
STM ΔsirA+F
STM ΔpflBΔsirA
STM ΔpflBΔsirA+F
N=3, n=3
C.
fliC
FOLD CHANGE (W.R.T WT)
STM WT
STM ΔsirA
STM ΔsirA+F
STM ΔpflBΔsirA
STM ΔpflBΔsirA+F
N=3, n=3
D.
fliC
FOLD CHANGE (W.R.T WT)
UT
+70
+90
+110
+150
STM WT
STM ΔpflB
N=3, n=3
F.
pflB
FOLD CHANGE (W.R.T Duodenum)
Duodenum
Ileum
N=3, n=3
G.
STM WT
SipC
DAPI
MERGED
STM ΔpflB
E.
INTRACELLULAR CONCENTRATION OF FORMATE
FOLD CHANGE IN INTRACELLULAR FORMATE (W.R.T UT STM WT)
UT
+40
+90
+110
STM WT
STM ΔpflB
N=4, n=2
H.
SipC
Normalized MFI
Duodenum
Ileum
STM WT
STM ΔpflB
n=7

991 **Figure 6**

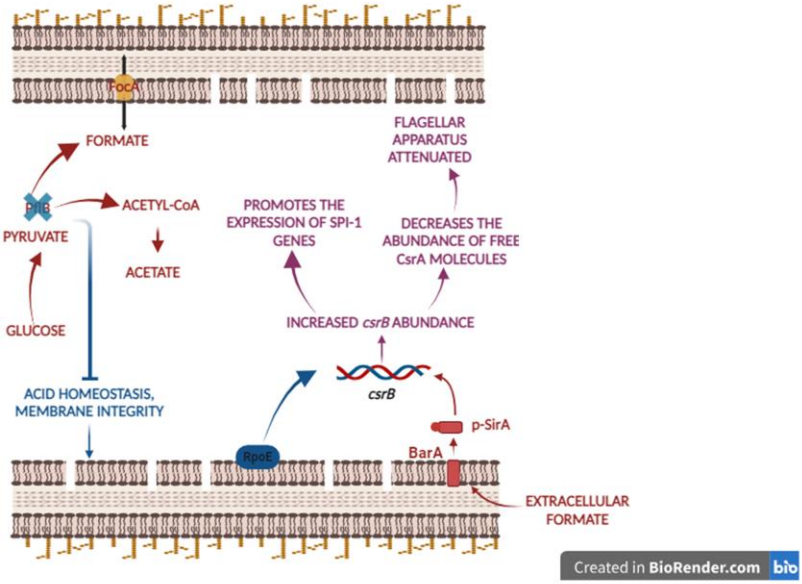

Graphical abstract

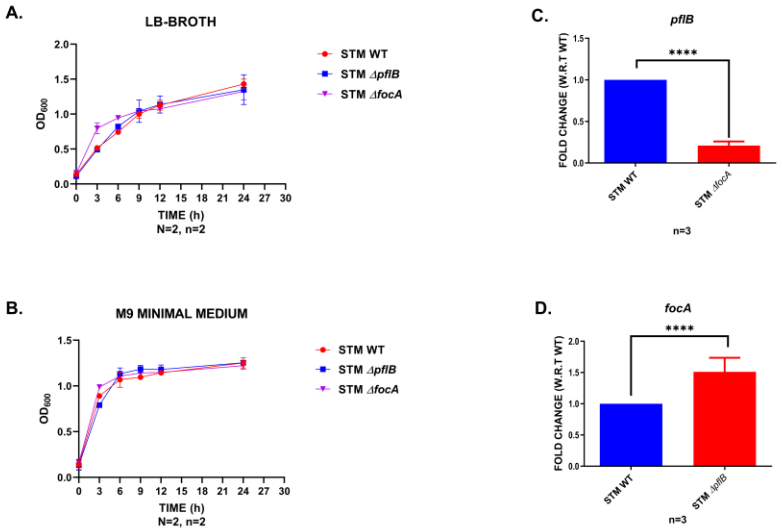

Supplementary Figure 1

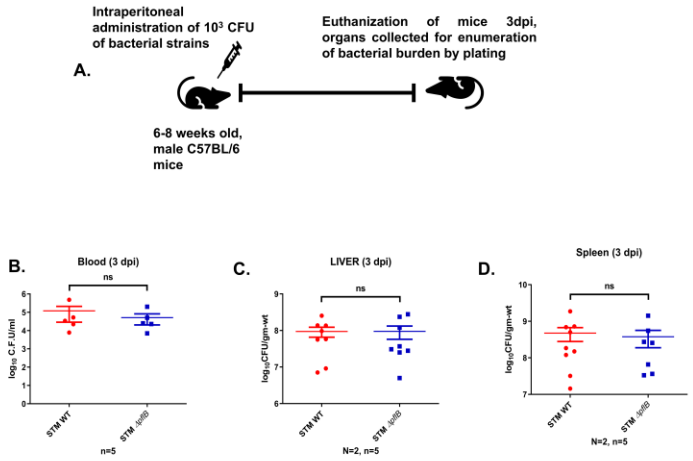

Supplementary Figure 2

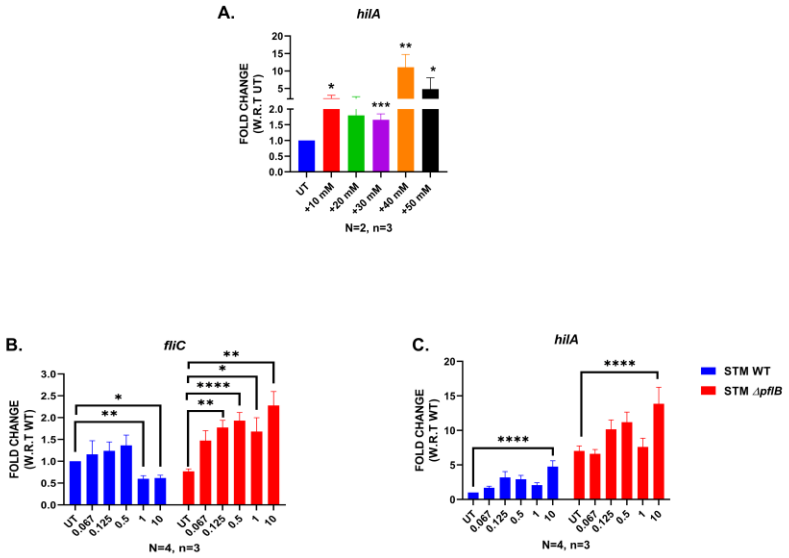

Supplementary Figure 3

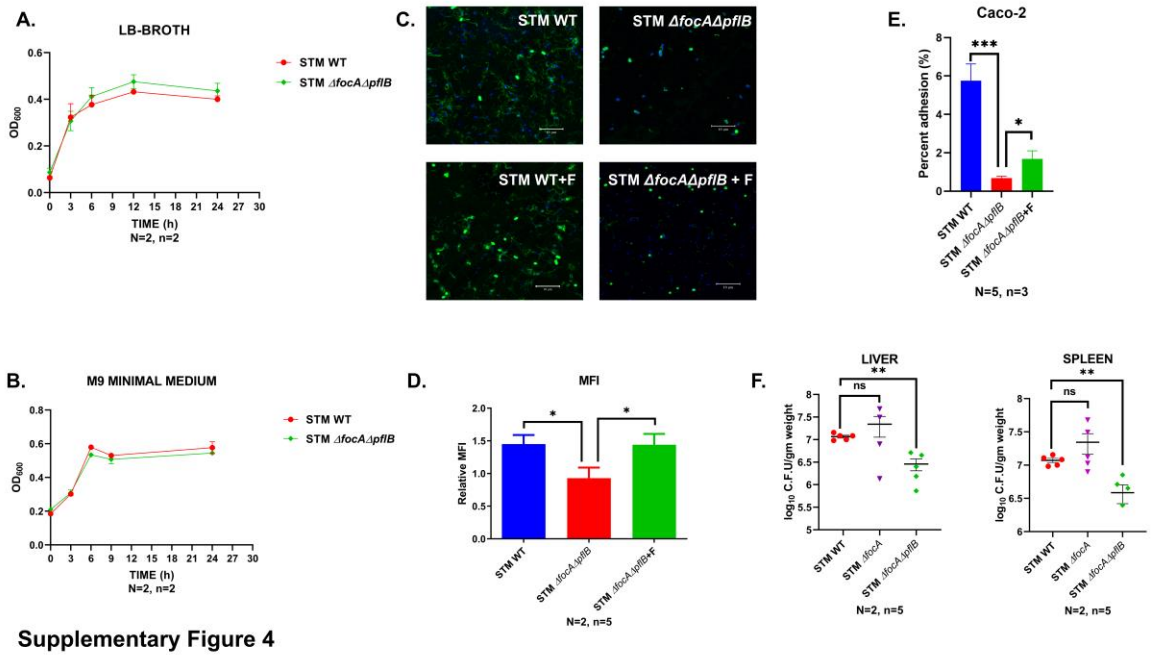

Supplementary Figure 4

997

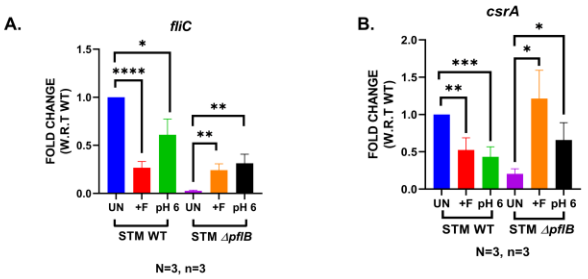

Supplementary Figure 5

998

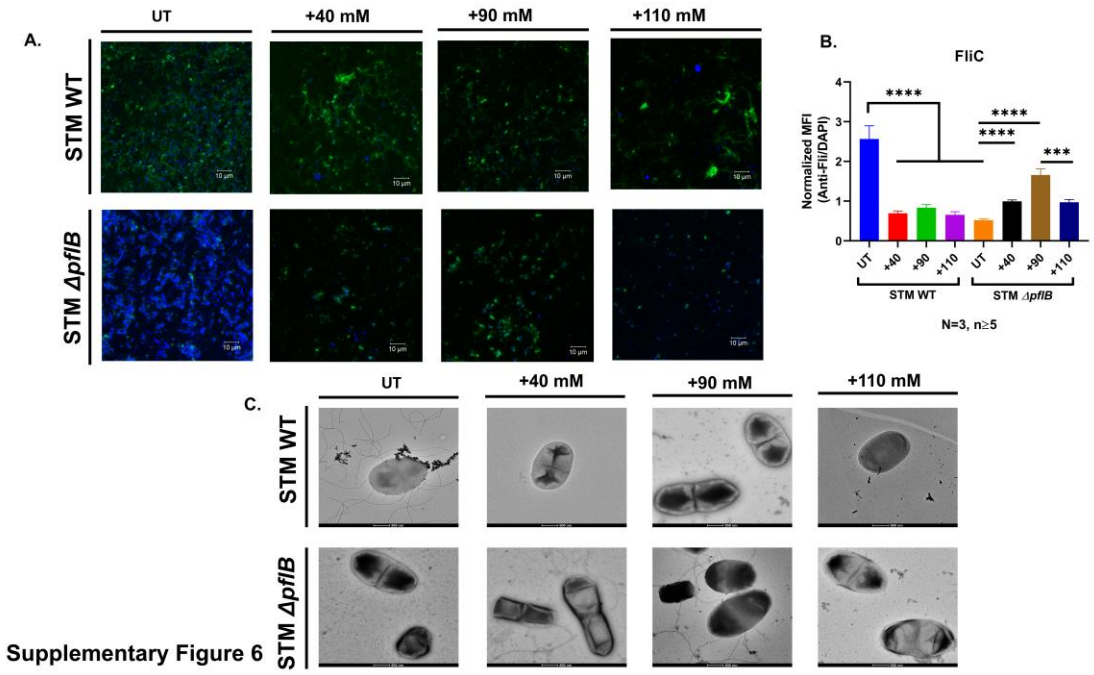

Supplementary Figure 6

Figure legends:

Figure 1: The deletion of the *pflB* gene led to decreased invasion efficiency in the Caco-2 cell line, which corresponded to a reduced organ burden in C57BL/6 mice five days after infection through oral gavaging

A. GC-MS mediated quantification of relative intracellular formate in STM WT, STM *ΔpflB*, STM *ΔfocA*, STM *ΔfocAΔpflB*. Data is represented as Mean+/-SEM of N=3, n=6.

B. GC-MS mediated quantification of residual formate in the spent media post incubation by STM WT, STM *ΔpflB*, STM *ΔfocA*, STM *ΔfocAΔpflB*. Data is represented as Mean+/-SEM of N=3, n=3.

C. Percent invasion of STM WT and STM *ΔpflB* in Caco-2 cell line. Data is represented as Mean+/-SEM of N=3, n=3.

1013 D. Fold proliferation of STM WT and STM *ΔpflB* in Caco-2 cell line. Data is represented
1014 as Mean+/-SEM of N=3, n=3.
1015 E. Percent phagocytosis of STM WT and STM *ΔpflB* in RAW 264.7 cell line. Data is
1016 represented as Mean+/-SEM of N=3, n=3.
1017 F. Fold proliferation of STM WT and STM *ΔpflB* in RAW 264.7 cell line. Data is
1018 represented as Mean+/-SEM of N=3, n=3.
1019 G. Schematic showing the protocol followed for invasion assay in C57BL/6 mice
1020 H. Bacterial burden in the intestine post 6h of infecting the mice with STM WT and STM
1021 *ΔpflB* via oral gavaging. Data is represented as Mean+/-SEM of N=2, n=5.
1022 I. Bacterial burden in the feces of mice post 6h of infection with STM WT and STM *ΔpflB*
1023 via oral gavaging. Data is represented as Mean+/-SEM of N=2, n=5.
1024 J. Schematic showing the protocol followed for determining the organ burden of STM
1025 WT and STM *ΔpflB* 5 days post oral gavaging
1026 K. Organ burden of STM WT and STM *ΔpflB* in liver 5 days post oral gavaging. Data is
1027 represented as Mean+/-SEM of N=3, n=5.
1028 L. Organ burden of STM WT and STM *ΔpflB* in spleen 5 days post oral gavaging. Data is
1029 represented as Mean+/-SEM of N=3, n=5.
1030 M. Survival rates of C57BL/6 mice post infection with STM WT and STM *ΔpflB* through
1031 oral route.

1032

1033 (Unpaired Student's t-test for column graphs, Two-way Anova for grouped data, Mann-
1034 Whitney U-test for animal experiment data (**** $p < 0.0001$, *** $p < 0.001$, ** $p<0.01$, *
1035 $p<0.05$))

1036

1037 **Figure 2: STM *ΔpflB* was deficient in flagella and the deficiency was recovered upon**
1038 **supplementation of formate**

1039 A. RT-qPCR mediated study of expression profile of *prgH* in the logarithmic phase
1040 cultures of STM WT, STM *ΔpflB* (+/-F). Data is represented as Mean+/-SEM of N=3,
1041 n=3.
1042 B. RT-qPCR mediated study of expression profile of *fliC* in the logarithmic phase cultures
1043 of STM WT, STM *ΔpflB* (+/-F). Data is represented as Mean+/-SEM of N=2, n=3.
1044 C. TEM assisted visualization of the flagellar structures in STM WT, STM *ΔpflB* (+/-F)
1045 D. Confocal microscopy assisted visualization of the flagellar structures in STM WT, STM
1046 *ΔpflB* (+/-F). Images are representative of N=2, n=5.
1047 E. Normalized Median Fluorescence Intensity (MFI), i.e.., MFI of Secondary antibody for
1048 Rabbit generated Anti-fli antibody/ MFI for DAPI in confocal microscopy assisted
1049 visualization of the flagellar structures in STM WT, STM *ΔpflB* (+/-F). Data is
1050 represented as Mean+/-SEM of N=2, n=5.
1051 F. Swim motility of STM WT and STM *ΔpflB* on 0.25% Agar containing LB plates
1052 G. Percent adhesion of STM WT, STM *ΔpflB*, STM *ΔfliC*(+/-F) in Caco-2 cell line. Data is
1053 represented as Mean+/-SEM of N=5, n=3.
1054 H. Percent invasion of STM WT, STM *ΔpflB*, STM *ΔpflB/*pQE60:*pflB* (+/-F) in Caco-2 cell
1055 line. Caco-2 cell line. Data is represented as Mean+/-SEM of N=2, n=2

1056 (Unpaired Student's t-test for column graphs, Two-way Anova for grouped data, Mann-
1057 Whitney U-test for animal experiment data (**** $p < 0.0001$, *** $p < 0.001$, ** $p<0.01$, *
1058 $p<0.05$))

1059

1060

1061 **Figure 3: STM *ΔpflB* had a higher intracellular pH and higher membrane depolarization,**
1062 **both of which were recovered upon formate supplementation**

1063 A. BCECF-AM dye mediated elucidation of the relative ipH in the logarithmic cultures of
1064 STM WT, STM *ΔpflB* (+/-F) in phosphate buffers of pH 5.5, 6, and 7. Data is
1065 represented as Mean+/-SEM of N=4, n=4.
1066 B. Elucidation of the ipH in the logarithmic cultures of STM WT/pBAD-pHuji and STM
1067 *ΔpflB*/pBAD-pHuji (+/-F). Data is represented as Mean+/-SEM of N=4, n=3.
1068 C. Bisbenzimide assay to quantify the membrane damage in the logarithmic cultures of
1069 STM WT, STM *ΔpflB,* STM *ΔfliC* (+/-F). Data is represented as Mean+/-SEM of N=6,
1070 n=5.
1071 D. Representative FACS percent positive and histogram profiles of $DiBAC_4$ staining in
1072 the logarithmic cultures of STM WT, STM *ΔpflB,* STM *ΔfliC* (+/-F). Data is
1073 representative of N=4, n=3.
1074 E. Flow cytometry obtained quantification of percent- $DiBAC_4$ positive cells in the
1075 logarithmic cultures of STM WT, STM *ΔpflB,* STM *ΔfliC* (+/-F) incubated in LB media
1076 (pH 7.2) and F-media (pH 5.5). Data is represented as Mean+/-SEM of N=4, n=3.

1077 (Unpaired Student's t-test for column graphs, Two-way Anova for grouped data, Mann-
1078 Whitney U-test for animal experiment data (**** $p < 0.0001$, *** $p < 0.001$, ** $p<0.01$, *
1079 $p<0.05$))

1080

1081 **Figure 4: STM *ΔpflB* had a higher transcript level of *csrB*, raising the possibility of**
1082 **flagella inhibition via the *csr* sRNA system**

1083 A. RT-qPCR mediated expression profile of the flagellar operon genes *flhD*, *flgA*, *flgK*,
1084 *fliA*, *motA* in the logarithmic cultures of STM WT, STM *ΔpflB (+/-F).* Data is
1085 represented as Mean+/-SEM of N=3, n=3.
1086 B. RT-qPCR mediated expression profile of the sRNA *csrB* in the logarithmic cultures of
1087 STM WT, STM *ΔpflB (+/-F).* Data is represented as Mean+/-SEM of N=6, n=3.
1088 C. RT-qPCR mediated expression profile of the *fliC* in the logarithmic cultures of STM
1089 WT and STM *ΔpflB* transformed with an pQE60*: csrA* under an IPTG-inducible system.
1090 Data is represented as Mean+/-SEM of N=3, n=3.
1091 D. Confocal microscopy assisted visualization of the flagellar structures in STM
1092 WT/pQE60: *csrA*, STM *ΔpflB*/pQE60: *csrA*. Images are representative of N=2, n=10.
1093 E. Normalized Median Fluorescence Intensity (MFI), i.e.., MFI of Secondary antibody for
1094 Rabbit generated Anti-fli antibody/ MFI for DAPI in confocal microscopy assisted
1095 visualization of the flagellar structures in STM WT/pQE60: *csrA*, STM *ΔpflB*/pQE60:
1096 *csrA*. Data is represented as Mean+/-SEM of N=2, n=10
1097 F. Percent adhesion of STM WT/pQE60: *csrA* and STM *ΔpflB*/pQE60: *csrA* in Caco-2
1098 cell line. Data is represented as Mean+/-SEM of N=3, n=3.
1099 G. TEM assisted visualization of the flagellar structures in STM WT/pQE60: *csrA*, STM
1100 *ΔpflB*/pQE60: *csrA.* Data is representative of N=2, n=10.

1101 (Unpaired Student's t-test for column graphs, Two-way Anova for grouped data, Mann-
1102 Whitney U-test for animal experiment data (**** $p < 0.0001$, *** $p < 0.001$, ** $p<0.01$, *
1103 $p<0.05$))

1104

1105 **Figure 5: The extra cytoplasmic sigma factor RpoE increases the expression of *csrB* and**
1106 **therefore restricts the expression of *fliC***

1107 A. RT-qPCR mediated expression profile of the sRNA *csrB* in the logarithmic cultures of
1108 STM WT, STM *ΔpflB*, STM *ΔrpoE*, STM *ΔpflBΔrpoE.* Data is represented as Mean+/-
1109 SEM of N=4, n=3.
1110 B. RT-qPCR mediated expression profile of the flagellar operon genes *flhD* and *fliC* in the
1111 logarithmic cultures of STM WT, STM *ΔpflB*, STM *ΔrpoE*, STM *ΔpflBΔrpoE*. Data is
1112 represented as Mean+/-SEM of N=2, n=3.
1113 C. Confocal microscopy assisted visualization of the flagellar structures in STM WT,
1114 STM *ΔpflB*, STM *ΔrpoE*, STM *ΔpflBΔrpoE*. Images are representative of N=2, n=10.
1115 D. Normalized Median Fluorescence Intensity (MFI), i.e.., MFI of Secondary antibody for
1116 Rabbit generated Anti-fli antibody/ MFI for DAPI in confocal microscopy assisted
1117 visualization of the flagellar structures in STM WT, STM *ΔpflB*, STM *ΔrpoE*, STM
1118 *ΔpflBΔrpoE*. Data is represented as Mean+/-SEM of N=2, n=10.
1119 E. TEM assisted visualization of the flagellar structures in STM WT, STM *ΔpflB*, STM
1120 *ΔrpoE*, STM *ΔpflBΔrpoE.* Data is representative of N=2, n=10.
1121 F. Swim motility of STM WT, STM *ΔpflB*, STM *ΔrpoE*, STM *ΔpflBΔrpoE* on 0.25% Agar
1122 containing LB plates
1123 G. Percent adhesion of STM WT, STM *ΔpflB*, STM *ΔrpoE*, STM *ΔpflBΔrpoE* in Caco-2
1124 cell line. Data is represented as Mean+/-SEM of N=2, n=3.

1125

1126 (Unpaired Student's t-test for column graphs, Two-way Anova for grouped data, Mann-
1127 Whitney U-test for animal experiment data (**** $p < 0.0001$, *** $p < 0.001$, ** $p<0.01$, *
1128 $p<0.05$))

1129

1130 **Figure 6: PflB maintains the switch between the flagellar expression and SPI-1 gene**
1131 **expression in intestine of the C57BL/6**

1132 A. RT-qPCR mediated expression profile of the SPI-1 genes *hilA* and *prgH* in the
1133 logarithmic cultures of STM WT, STM *ΔpflB*, STM *ΔrpoE*, STM *ΔpflBΔrpoE.* Data is
1134 represented as Mean+/-SEM of N=4, n=3.
1135 B. RT-qPCR mediated expression profile of the SPI-1 genes *hilA* and *prgH* in the
1136 logarithmic cultures of STM WT, STM *ΔpflB*, STM *ΔsirA*, STM *ΔpflBΔsirA.* Data is
1137 represented as Mean+/-SEM of N=4, n=3.
1138 C. RT-qPCR mediated expression profile of *fliC* gene in the logarithmic cultures of STM
1139 WT, STM *ΔpflB*, STM *ΔrpoE*, STM *ΔpflBΔrpoE.* Data is represented as Mean+/-SEM
1140 of N=3, n=3.
1141 D. RT-qPCR mediated expression profile of *fliC* gene in the logarithmic cultures of STM
1142 WT and STM *ΔpflB* supplemented with 70, 90, 110, 150 mM of sodium formate. Data
1143 is represented as Mean+/-SEM of N=3, n=3.
1144 E. GC-MS mediated quantification of relative intracellular formate in STM WT, STM
1145 *ΔpflB*, supplemented with 40, 90, 110 mM Sodium formate. Data is represented as
1146 Mean+/-SEM of N=4, n=2
1147 F. RT-qPCR mediated expression profile of *pflB* gene in the duodenum and ileum of the
1148 intestine of C57BL/6 mice. Data is represented as Mean+/-SEM of N=3, n=3.
1149 G. Confocal microscopy assisted visualization of the SPI-1 effector SipC protein in the
1150 duodenum and ileum of mice infected with STM WT and STM *ΔpflB*. Images are
1151 representative of n=7.
1152 H. Confocal microscopy assisted visualization of the SPI-1 effector SipC protein in the
1153 duodenum and ileum of mice infected with STM WT and STM *ΔpflB*. Images are
1154 representative of n=7.

1155

1156 (Unpaired Student's t-test for column graphs, Two-way Anova for grouped data, Mann-
1157 Whitney U-test for animal experiment data (**** $p < 0.0001$, *** $p < 0.001$, ** $p<0.01$, *
1158 $p<0.05$))

1159

1160 **Supplementary Figure 1: STM *ΔpflB*, and STM *ΔfocA* are not growth deficient in LB**
1161 **Broth, M9 Minimal Media. Deletion of pflB caused an enhanced expression of *focA***

1162 A. Growth curves of STM WT, STM *ΔpflB* and STM *ΔfocA* in LB broth, M9 Minimal
1163 Media. Data is represented as Mean+/-SEM of N=2, n=2.
1164 B. Growth curves of STM WT, STM *ΔpflB* and STM *ΔfocA* in M9 Minimal Media. Data
1165 is represented as Mean+/-SEM of N=2, n=2.
1166 C. RT-qPCR mediated expression profile of *pflB* gene in the logarithmic cultures of STM
1167 *ΔfocA*. Data is represented as Mean+/-SD of n=3.
1168 D. RT-qPCR mediated expression profile of *focA* gene in the logarithmic cultures of STM
1169 *ΔpflB*. Data is represented as Mean+/-SD of n=3.

1170 (Unpaired Student's t-test for column graphs, Two-way Anova for grouped data, Mann-
1171 Whitney U-test for animal experiment data (**** $p < 0.0001$, *** $p < 0.001$, ** $p<0.01$, *
1172 $p<0.05$))

1173

1174 **Supplementary Figure 2: Intraperitoneal infection of STM WT and STM *ΔpflB* lead to**
1175 **no significant change in the bacterial burden in blood, liver, and spleen 3 dpi**

1176 A. Schematic showing the protocol followed for determining the organ burden of STM WT
1177 and STM *ΔpflB* 3 days post intraperitoneal infection

1178 B-D. Bacterial burden of STM WT and STM *ΔpflB* in blood (B), liver (C), and spleen. Data is
1179 represented as Mean+/-SEM of N=2, n=5.

1180 (Unpaired Student's t-test for column graphs, Two-way Anova for grouped data, Mann-
1181 Whitney U-test for animal experiment data (**** $p < 0.0001$, *** $p < 0.001$, ** $p<0.01$, *
1182 $p<0.05$))

1183

1184 **Supplementary Figure 3: Formate modulates the expression of *fliC* and *hilA* in STM WT**
1185 **and STM *ΔpflB* in a concentration dependent manner.**

1186 A. Expression of *hilA* in STM WT in formate supplemented at concentrations of 10, 20,
1187 30, 40, and 50 mM. Data is representative of N=2, n=3 and expressed as Mean+/- SD.
1188 B. Expression of *fliC* in STM WT and STM *ΔpflB* in formate supplemented at
1189 concentrations of 0.067, 0.125, 0.5, 1, 10 mM. Data is represented as Mean+/-SEM of
1190 N=4, n=3.
1191 C. Expression of *hilA* in STM WT and STM *ΔpflB* in formate supplemented at
1192 concentrations of 0.067, 0.125, 0.5, 1, 10 mM. Data is represented as Mean+/-SEM of
1193 N=4, n=3.

1194 (Unpaired Student's t-test for column graphs, Two-way Anova for grouped data, Mann-
1195 Whitney U-test for animal experiment data (**** $p < 0.0001$, *** $p < 0.001$, ** $p<0.01$, *
1196 $p<0.05$))

1197

1198 **Supplementary Figure 4: STM *ΔfocAΔpflB* had an attenuated flagellar apparatus, with**
1199 **partial recovery upon supplementation of extragenous F**

1200 A. Growth curves of STM WT, STM *ΔfocAΔpflB* in LB broth and M9 Minimal Media.
1201 Data is represented as Mean+/-SEM of N=2, n=2.
1202 B. Growth curves of STM WT, STM *ΔpflB* and STM *ΔfocA* in M9 Minimal Media. Data
1203 is represented as Mean+/-SEM of N=2, n=2.
1204 C. Confocal microscopy assisted visualization of the flagellar structures in STM WT, STM
1205 *ΔfocAΔpflB* (+/-F). Images are representative of N=2, n=5.
1206 D. Normalized Median Fluorescence Intensity (MFI), i.e.., MFI of Secondary antibody for
1207 Rabbit generated Anti-fli antibody/ MFI for DAPI in confocal microscopy assisted
1208 visualization of the flagellar structures in STM WT, STM *ΔfocAΔpflB* (+/-F). Data is
1209 represented as Mean+/-SEM of N=2, n=5.
1210 E. Percent adhesion of STM WT and STM *ΔfocAΔpflB* in Caco-2 cell line. Data is
1211 represented as Mean+/-SEM of N=5, n=3.
1212 F. Organ burden of STM WT and STM *ΔfocAΔpflB* in liver and spleen of C57BL/6 mice
1213 5 days post oral gavaging. Data is represented as Mean+/-SEM of N=2, n=5.

1214 (Unpaired Student's t-test for column graphs, Two-way Anova for grouped data, Mann-
1215 Whitney U-test for animal experiment data (**** $p < 0.0001$, *** $p < 0.001$, ** $p<0.01$, *
1216 $p<0.05$))

1217

1218 **Supplementary Figure 5: Decreased expression of *fliC* in STM *ΔpflB* can be altered upon**
1219 **incubating the bacterial cultures in acidic media (pH of 6).**

1220 **A.** RT-qPCR mediated expression profile of *fliC* in the logarithmic cultures of STM WT,
1221 STM *ΔpflB* incubated in acidic LB media (pH 6). Data is represented as Mean+/-SEM
1222 of N=3, n=3.

1223 **B.** RT-qPCR mediated expression profile of *csrA* in the logarithmic cultures of STM WT,
1224 STM *ΔpflB* incubated in acidic LB media (pH 6). Data is represented as Mean+/-SEM
1225 of N=3, n=3.

1226 (Unpaired Student's t-test for column graphs, Two-way Anova for grouped data, Mann-
1227 Whitney U-test for animal experiment data (**** $p < 0.0001$, *** $p < 0.001$, ** $p<0.01$, *
1228 $p<0.05$))

1229

1230

1231 **Supplementary Figure 6: Compensation of intracellular formate pool in STM *ΔpflB***
1232 **makes it mimic the behaviour of STM WT**

1233 A. Confocal microscopy assisted visualization of the flagellar structures in STM WT, STM
1234 *ΔpflB* supplemented with 40, 90, 110 mM of sodium formate. Images are representative
1235 of N=3, n≥5.
1236 B. Normalized Median Fluorescence Intensity (MFI), i.e.., MFI of Secondary antibody for
1237 Rabbit generated Anti-fli antibody/ MFI for DAPI in confocal microscopy assisted
1238 visualization of the flagellar structures in STM WT, STM *ΔpflB* supplemented with 40,
1239 90, 110 mM of sodium formate. Data is represented as Mean+/-SEM of N=3, n≥5.
1240 C. TEM assisted visualization of the flagellar structures in STM WT and STM *ΔpflB*
1241 supplemented with 40, 90, 110 mM of sodium formate. Data is representative of N=2,
1242 n=10.